Divalent siRNA for prion disease

Juliana E Gentile[1], Taylor L Corridon[1], Dimas Echeverria[2], Fiona E Serack[1], Zachary E Kennedy[2*], Corrie L Gallant-Behm[3], Matthew R Hassler[3], Garth Kinberger[3], Nikita G Kamath[1], Katherine Y Gross[2], Yuan Lian[1], Rachael Miller[2], Kendrick DeSouza-Lenz[4], Michael Howard[4], Kenia Guzman[4], Nathan Chan[4], Vanessa Laversenne[1], Daniel T Curtis[3**], Kevin Fettes[5], Marc Lemaitre[6], Gregg Cappon[7], Aimee L Jackson[3], Ken Yamada[2], Julia F Alterman[2], Alissa A Coffey[1], Eric Vallabh Minikel[1,8,9,10†], Anastasia Khvorova[2†], Sonia M Vallabh[1,8,9,10†]

1. Program in Brain Health, Broad Institute of MIT and Harvard, Cambridge, MA, 02142, USA
2. RNA Therapeutics Institute, UMass Chan Medical School, Worcester, MA, 01655, USA
3. Atalanta Therapeutics, Boston, MA, 02210, USA
4. Comparative Medicine, Broad Institute of MIT and Harvard, Cambridge, MA, 02142, USA
5. FTS Pharma Consulting, Medfield, MA, 02052, USA
6. ML Consult LLC
7. Tox Strategies, Asheville, NC, 28801, USA
8. McCance Center for Brain Health and Department of Neurology, Massachusetts General Hospital, Boston, MA, 02114, USA
9. Department of Neurology, Harvard Medical School, Boston, MA, 02115, USA
10. Prion Alliance, Cambridge, MA, 02139, USA

*Present address: CANbridge Pharmaceuticals, Burlington, MA 01803, USA
**Present address: Stealth biotech startup, Boston, MA 02114 USA
†Correspondence to: eminikel@broadinstitute.org, anastasia.khvorova@umassmed.edu, or svallabh@broadinstitute.org

Abstract

Pharmacologic lowering of PrP expression is efficacious against prion disease in animal models and is now being tested clinically. 50% lowering of PrP increases both survival time and healthy life in prion-infected mice, but does not prevent symptom onset nor halt disease progression. Additional drug candidates should seek to reduce PrP expression to even lower levels. Divalent siRNA is a novel oligonucleotide drug modality with promising potency, durability, and biodistribution data in preclinical models, inspiring us to seek in this technology a new drug candidate for prion disease. Here, we first identify a tool compound against the mouse PrP gene and establish the efficacy of PrP-lowering divalent siRNA in prion-infected mice. We then introduce humanized transgenic mouse lines harboring the full non-coding sequence of the human PrP gene as tools for identifying human sequence-targeted drugs. We identify a highly potent siRNA sequence against the human PrP gene and determine that a chemical scaffold incorporating extended nucleic acid and a 3′ antisense tail unmatched to the RNA target yields superior potency. We nominate PrP-lowering divalent siRNA 2439-s4 as a new drug candidate for human prion disease.

Introduction

Prion disease is a fatal, incurable neurodegenerative disease caused by misfolding of prion protein (PrP), encoded in humans by the gene *PRNP*[1]. Convergent lines of evidence implicate PrP as the drug target in this disease[2], and indicate that lowering PrP should be both safe[3–9] and effective[10–15]. PrP-lowering antisense oligonucleotides (ASOs) both delay onset and slow progression of prion disease in mice[16–18], which has led to an ongoing Phase I/II clinical trial of an intrathecal PrP-lowering ASO, ION717, in symptomatic patients with prion disease (NCT06153966).

We seek to augment the therapeutic pipeline for prion disease, for several reasons. Only 8-14% of drug candidates that enter Phase I ultimately reach approval[19–21], and while drug targets backed by human genetic evidence enjoy increased success rates[22], even these targets may take many drug candidates and many trials to yield a success[23]. In mice, lowering by approximately half via heterozygous knockout or chronic early ASO treatment prolongs survival up to 3-fold, but all mice ultimately succumb to fatal prion disease[18], consistent with prion replication continuing, albeit at a reduced rate[24]. Thus, to halt or indefinitely delay prion disease will require deeper than 50% target lowering.

We sought to develop a divalent siRNA drug candidate for prion disease. Like ASOs, siRNAs are chemically modified oligonucleotide drugs that bind a target RNA through Watson-Crick base pairing, but whereas ASOs recruit RNase H1 to cleave the target RNA[25], siRNAs engage the RNA Induced Silencing Complex (RISC) to cleave their target[26]. Like ASOs, siRNAs accumulate in endosomal depots[27], and their slow release from this compartment combined with their chemical stabilization allows them to provide months of pharmacologic effect following a single dose into cerebrospinal fluid (CSF). Divalent siRNA[28] is a novel siRNA architecture designed to enhance gene silencing within the central nervous system (CNS). It consists of two fully chemically modified siRNA molecules connected by a linker, forming a larger molecule that distributes broadly in the brain following direct delivery into cerebrospinal fluid (CSF) and potently lowers its target RNA. Inspired by deep lowering of *HTT, APOE,* and *SOD1* in the rodent CNS[28–30], we set out to identify potent reagents against *PRNP* and to improve upon the divalent siRNA technology. Divalent siRNA incorporates a variable number of phosphorothioate (PS) linkages at the 5′ and 3′ ends of each strand; PS is vital for cellular uptake and durability of oligonucleotide drugs but also mediates at least some toxicological properties, at least for single-stranded oligonucleotides[31,32]. We therefore also tested the hypothesis that the recently reported highly nuclease-resistant extended nucleic acid (exNA) nucleotide linkage[33] would permit us to reduce the number of PS linkages. In addition, because full complementarity to target RNA can result in RISC unloading or siRNA degradation[34,35], we also sought to test the hypothesis that a fixed, non-complementary 3′ tail at the end of the antisense (AS) strand would improve potency.

Herein, we identify a modestly potent tool compound against mouse *Prnp* and demonstrate that ~50% PrP lowering with this new modality extends survival in prion-infected wild-type mice, replicating work with ASOs. We develop transgenic human *PRNP* mouse models and use them

to identify a highly potent drug candidate against human *PRNP*, yielding as little as 17% residual PrP in whole brain hemisphere after a single dose. We demonstrate that a fixed tail and a reduced phosphorothioate AS strand with exNA linkages improve potency. We find activity out to 6 months post-dose and characterize the effect of repeat dosing on target engagement. Ultimately, we nominate a new drug candidate for prion disease.

Methods

Oligonucleotide synthesis — UMass

Oligonucleotides were synthesized by phosphoramidite solid-phase synthesis on automated synthesizer using a MerMade12 (Biosearch Technologies, Novato, CA), Dr Oligo 48 (Biolytic, Fremont, CA) or AKTA Oligopilot 100 (Cytiva, Marlborough, MA). 5′-(E)-Vinyl tetraphosphonate (pivaloyloxymethyl) 2′-O-methyl-uridine 3′-CE phosphoramidite was used for the addition of 5′-Vinyl Phosphonate, 2'-F, 2'-OMe phosphoramidites with standard protecting groups were used to make the modified oligonucleotides. Phosphoramidites were dissolved at 0.1 M in anhydrous acetonitrile (ACN), with added anhydrous 15% dimethylformamide in the case of the 2′-OMe-Uridine amidite. 5-(Benzylthio)-1H-tetrazole (BTT) was used as the activator at 0.25 M. Coupling times were 4 minutes. Detritylations was performed using 3% trichloroacetic acid in dichloromethane or Toluene. Capping reagents used were CAP A (20% N-methylimidazole in ACN) and CAP B (20% acetic anhydride and 30% 2,6-lutidine in ACN). Phosphite oxidation to convert to phosphate or phosphorothioate was performed with 0.05 M iodine in pyridine-water (9:1, v/v) or 0.1 M solution of 3-[(dimethylaminomethylene)amino]-3H-1,2,4-dithiazole-5-thione (DDTT) in pyridine for 3 min, respectively. All reagents were purchased from Chemgenes, Wilmington, MA, phospohoramidites were purchased from Chemgenes and Hongene Biotech, Union City, CA. Oligonucleotides were grown on long-chain alkyl amine (LCAA) controlled pore glass (CPG) functionalized via succinyl linker with either Unylinker terminus for unconjugated oligonucleotides 500Å (Chemgenes), with cholesterol through a tetraethylene glycol linker 500Å (Chemgenes), or with a di-trityl protected support separated by a tetraethylene glycol linker 1000Å (Hongene Biotech) for divalent sense oligonucleotides.

For in cellulo experiments, oligonucleotides with or without cholesterol conjugate were cleaved and deprotected on-column with Ammonia gas (Airgas Specialty Gases). Briefly, columns were pre-wet with 100uL of water and immediately spun to remove the excess water. Columns were then placed in a reaction chamber (Biolytic) 90min at 65°C. A modified on-column ethanol precipitation protocol was used for desalting and counterion exchange. Briefly, 1mL of 0.1M sodium acetate in 80% ethanol is flushed through the column, followed by a rinse with 1mL 80% ethanol and finally after drying the excess ethanol, oligonucleotides were eluted with 600uL of water in 96 deep well plates.

For in vivo experiments, 5′-(E)-Vinyl-phosphonate containing oligonucleotides were cleaved and deprotected with 3% diethylamine in ammonium hydroxide, for 20 h at 35℃ with agitation. Divalent oligonucleotides were cleaved and deprotected with 1:1 ammonium hydroxide and 40%

aqueous monomethylamine, for 2 h at 25℃ with slight agitation. The controlled pore glass was subsequently filtered and rinsed with 30 mL of 5% ACN in water and dried overnight by centrifugal vacuum concentration. Purifications were performed on an Agilent 1290 Infinity II HPLC system using Source 15Q anion exchange resin (Cytiva). The loading solution was 20 mM sodium acetate in 10% ACN in water, and elution solution was the loading solution with 1M sodium bromide. Both oligonucleotide strands were eluted using a linear gradient from 30 to 70% in 40 min at 50°C. Peaks were monitored at 260nm. Pure fractions were combined and desalted by size exclusion using Sephadex G-25 resins (Cytiva). Oligonucleotides were then lyophilized and resuspended in water.

Purity and identity of oligonucleotides were confirmed by IP-RP HPLC coupled to an Agilent 6530 Accurate-mass Q-TOF. LC parameters: buffer A: 100 mM 1,1,1,3,3,3-hexafluoroisopropanol (HFIP) (Oakwood Chemicals) and 9 mM triethylamine (TEA) (Fisher Scientific) in LC–MS grade water (Fisher Scientific); buffer B:100 mM HFIP and 9 mM TEA in LC–MS grade methanol (Fisher Scientific); column, Agilent AdvanceBio oligonucleotides C18; linear gradient 5–35% B 5min was used for unconjugated and divalent oligonucleotides; linear gradient 25–80% B 5min was used for cholesterol conjugated oligonucleotides; temperature, 60°C; flow rate, 0.85 ml/min. Peaks were monitored at 260nm. MS parameters: Source, electrospray ionization; ion polarity, negative mode; range, 100–3,200 m/z; scan rate, 2 spectra/s; capillary voltage, 4,000; fragmentor, 200 V; gas temp, 325°C.

Initial screen for human and mouse siRNA sequences.

Screening of siRNA sequences in cellulo utilized monovalent cholesterol tetraethylene glycol (Chol-TEG) conjugated siRNAs, as cholesterol conjugates have demonstrated efficient gymnotic uptake into cultured cells and utility as tools for screening[36]. The initial screening for potent siRNA sequences was conducted at UMass Chan, including both the synthesis of siRNAs in the monovalent **Chol-TEG s1** scaffold (Figure S1) and the cell culture screening experiments. Sense and antisense oligonucleotides were annealed together at 95°C for 10 minutes and then cooled to room temperature. Screens were performed in N2a cells (mouse; ATCC No. CCL-131) or A549 cells (human; ATCC No. CCL-185). Cells were seeded into triplicate wells with growth media containing 1.5 μM of compound. After 72 hours, cell lysates were harvested. Mouse *Prnp* / human *PRNP* RNA were quantified with Quantigene assays (QGS-1000 SB-3030881 and SA-3002866 respectively), and as housekeeping controls, *Hprt/HPRT* RNA were quantified (assays SB-15463 and SA-10030 respectively) using the QuantigeneTM 2.0 branched DNA assay (Invitrogen). The ratio of *Prnp/PRNP* to *Hprt/HPRT* was normalized to the mean of expected non-targeting sequences (meaning, data for human cells were normalized to the mean of mouse-only sequences, while data for mouse cells were normalized to the mean of human-only sequences) to obtain an estimate of residual target expression after siRNA treatment. Highly active compounds found in the screen were then assayed in triplicate across 7 doses (23 nM – 1.5 μM) to calculate half-maximal inhibitory concentration (IC_{50}). The numbering of human siRNA sequences used herein is relative to the transcription start site of a now-outdated RefSeq transcript NM_000311.4, though we note that

human brain expression data support exclusive use of canonical Ensembl transcript ENST00000379440.9 which begins 362 bases further downstream[37].

Expanded screen for potent human siRNA sequences.

Further screening for potent human siRNA sequences was conducted with siRNAs synthesized in the monovalent **Chol-TEG s2** scaffold at Atalanta Therapeutics and tested in cellulo at the Broad Institute. Oligonucleotides were synthesized with standard solid-support phosphoramidite chemistry using a Dr. Oligo synthesizer. For single point primary screens siRNAs were diluted to twice the desired final concentration in optiMEM (Gibco cat no: 31985070) and for IC50 determination a 9- point 1:3 serial dilution series was used. U-251 MG glioblastoma cells (Sigma Aldrich cat no: 09063001) growing in a T75 flask were washed with PBS, trypsinized then quenched with growth media: optiMEM, 10% FBS, 1% NEAA (Gibco cat no: 11140050), 1% GlutaMAX (Gibco cat no: 35050061), 1% pen/strep (Gibco cat no: 15140122). Cells were pelleted at 1000 rpm for 5 minutes, growth media was aspirated then cells were resuspended in media containing 6% FBS without pen/strep. Sterile PBS was placed in outer wells of a 96-well plate to limit evaporation, while 8,000 cells per well were plated on the inner 60 wells. 50 µL of prepared cells was added to every well. 50 µL of optiMEM with 2x siRNA was added to the treated wells. Every plate contained 6-wells of “untreated cells” (50 µL optiMEM with no additives) for assay normalization purposes. After 72 hrs, any wells with cell death or rounded cells were noted then cells were lysed using the Cells-to-CT 1-step TaqMan Kit (Invitrogen cat no: A25602) according to the manufacturer protocol, with slight deviations. Media was aspirated from all wells then cells were washed with 200 µL 4°C sterile PBS. PBS was aspirated from every well before adding lysis solution containing DNase. Plate was placed on a shaker for 5 minutes then stop solution was added to every well. Cells were placed back on a shaker for 3 minutes then RNA was stored. RT-PCR samples were prepared using Taqman 1-Step qRT-PCR master mix and Taqman gene expression assays for human *TBP* (Invitrogen, cat no: Hs00427620_m1) and human *PRNP* (Invitrogen, cat no: Hs00175591_m1). Samples were run on a QuantStudio 7 Flex system (Applied Biosystems) using the following cycling conditions: reverse transcription 50°C, 5 min; reverse transcription inactivation/initial denaturation 95°C, 20 s; amplification 95°C, 3 s, 60°C, 30 s, 40 cycles. Each biological sample was run in duplicate, and the level of all targets were determined by ΔΔCt whereby results were first normalized to the housekeeping gene TBP and then to the untreated samples.

In silico off-targets analysis

The reverse complement of bases 2-17 of the 2439-exNA sequence — CACTTTGTGAGTATTC — was searched in NCBI Nucleotide BLAST (https://blast.ncbi.nlm.nih.gov/Blast.cgi) with the following settings. Database: Standard databases (nr etc.): > RefSeq Select RNA sequences (refseq_select). Organism: Homo sapiens (taxid:9606). Optimize for: Highly similar sequences (megablast). Max target sequences: 5,000. Match/mismatch scores: 1,-1. All other settings default. The top 100 hits from BLAST were downloaded as an XML file and parsed into tabular form using a Python script generated by ChatGPT. The table was then filtered using a custom R

script to include only matches where the search string was antisense to the target, consistent with the siRNA mechanism, and was sorted by number of mismatches.

Transgenic mouse generation

Transgenesis was performed by Cyagen (Santa Clara, CA) at its site in Taicang, Jiangsu, China. Searching NCBI CloneDB nominated bacterial artificial chromosome (BAC) RP11-715K24 as overlapping human PRNP. After sequence confirmation, *PRNP* and flanking sequence were cloned into the pStart-K plasmid by gap-repair cloning, with the p15A origin of replication and kanamycin resistance cassette located downstream of the gene, yielding a 48kb plasmid whose sequence is provided in this study's online git repository. The plasmid was linearized with restriction enzyme NruI and microinjected into fertilized C57BL/6 eggs. PCR screening identified four founder pups, of which animals 26372 (male) and 25109 (female) were successfully bred. Transgenic animals were backcrossed to wild-type C57BL/6N animals until generation F5, then crossed to ZH3 PrP knockout mice[38] (on a C57BL/6J background) housed at McLaughlin Research Institute, with rederivation to remove opportunistic pathogens performed by Charles River Labs.

Transgene characterization

Transgene mapping was performed by Taconic and Cergentis using targeted locus amplification (TLA)[39] on spleens from 9-week-old males of generation F3 (Tg26372) and F6 (Tg25109). TLA utilized primer sets shown in Table S25. Copy number was estimated based on the number of transgene-transgene fusion reads and the ratio of transgene coverage to flanking region coverage. Full transgene characterization reports are provided in this study's online git repository. Sequencing of the Tg26372 mouse utilized custom capture probes by Twist Bioscience targeting 152kb of human sequence surrounding PRNP as previously described[40]. Zygosity-aware genotyping was performed by Transnetyx.

Dose levels of siRNA

Drugs were formulated to target doses in terms of nanomoles (nmol) total bilateral dose, with the molarity referring to the full divalent siRNA molecule and not the monovalent equivalents. We targeted dose levels of 10, 5, 1.5, 1, or 0.2 nmol, based on siRNA concentrations determined by UV absorbance on NanoDrop. At UMass Chan, concentration determinations initially used the theoretical molar extinction coefficients (MECs) determined by the base composition method, in which the extinction coefficients of each base are summed and multiplied by 0.9 to account for base stacking. For instance, for our drug candidate 2439-s4, we formulated drug for mouse studies based on the theoretical MEC of 766,260 $L \cdot mol^{-1} \cdot cm^{-1}$ (twice the sum of the antisense and sense strand MECs). The theoretical base composition MECs, however, do not account for hypochromicity — oligonucleotides absorb less UV light when duplexed. At Atalanta, the nearest-neighbors (NN) was used, which attempts to account for the hyperchromicity in a sequence-specific manner. For 2439-s2, this yielded a theoretical MEC of 656,658 $L \cdot mol^{-1} \cdot cm^{-1}$. Later in the development program the MEC of 2439-s4 was determined

empirically to be 549,107 $L \cdot mol^{-1} \cdot cm^{-1}$. This indicated that all doses of compounds synthesized at UMass Chan had been 1.395 times higher than believed at the time. Thus, for instance, studies of 2439-s4 conducted at a 10 nmol dose were in fact at 13.95 nmol. An empirical MEC for 2439-s2 was never determined. The 13.95 nmol dose, multiplied by the 2439-s4 molecular weight of 24,952 Da, corresponds to 348 µg. Although empirical MECs were not determined for any other compounds tested here, we applied this same correction factor across all compounds described herein. Thus, the tested dose levels of 10, 5, 1.5, 1, or 0.2 nmol are estimated to correspond respectively to 348, 174, 52, 35, and 7 µg. We note that if the hypochromicity of the s2 compounds synthesized at Atalanta is similar to that of 2439-s4, then the doses of Atalanta compounds tested herein may actually be 14% lower than those of UMass Chan compounds.

Animal studies

All animal studies were conducted under Broad Institute IACUC protocol 0162-05-17. Transgenic mice (see above) were bred at the Broad Institute. Wild-type C57BL/6N mice were purchased from Charles River Laboratories.

Administration of divalent siRNA to mice

For in vivo use, siRNAs were synthesized in divalent format by UMass Medical School or Atalanta Therapeutics, see detailed methods above. Atalanta compounds were formulated in 1X PBS without ionic conditioning. At UMass Chan, to prevent neurotoxicity due to divalent cation imbalance[41,42] ionic conditioning was employed: stock solutions of 1 mM divalent siRNA (2 mM monovalent equivalents) were prepared with 2 mM $MgCl_2$, 14 mM $CaCl_2$, 8 mM HEPES, 20 mM D-glucose, 5 mM KCl, and 137 mM NaCl. Dilutions of this stock were prepared in artificial CSF containing 137 mM NaCl, 5 mM KCl, 20 mM D-glucose, and 8 mM HEPES. siRNAs were delivered to mice via bilateral intracerebroventricular (ICV) injection, 5 µL per side for a total of 10 µL injection volume. The ICV procedure was slightly modified from that described previously for antisense oligonucleotides[18]. In the first 4 in vivo target engagement studies, animals were anesthetized with 1.2% tribromoethanol, injected i.p. with 0.23 mL per 10 g of body weight using an insulin syringe (BD 329410). Tribromoethanol was prepared freshly each week according to a published protocol[43], passed through a 0.22 µm filter, handled under sterile conditions and stored at 4°C in the dark until use, discarding if stored past 2 weeks. In the remaining 12 in vivo target engagement studies and in the survival studies in the prion disease model, we used 3% isoflurane inhalation anesthesia. Anesthetized animals were immobilized in a stereotactic apparatus (SAS-4100, ASI Instruments) with 18° ear bars and the nose bar set to -8 mm. Heads were shaved and scalps swabbed with povidone/iodine and alcohol swabs, a 1 cm incision was made along the midline and the periosteum was scrubbed with a sterile cotton-tipped applicator to reveal the bregma landmark. Microliter syringes with either 26G or 22G needles (Hamilton company model 701, point style 2, No. 80300 or 80308 respectively) were filled with 10 µL of formulated drug or vehicle. From bregma, the needle was moved 0.3 mm rostral, 1.0 mm right or left, then down until it touched the skull and then 3.5 mm ventral. 5 µL was ejected gradually

over ~10 seconds, then after a 1 minute pause the needle was backed out while maintaining downward pressure on the skull with a cotton-tipped applicator. This procedure was performed first on the right and then on the left. After both injections, incisions were closed with either wound clips (Braintree Scientific cat no: RF7) or sutured with a single horizontal mattress stitch (Ethicon 661H). In target engagement studies, animals were generally harvested after 4 weeks, and a minimum of 3 weeks, in-life, to permit a sufficient number of PrP half-lives to observe lowering at the protein level[44].

Prion infection

Prion inoculations were performed as described previously[17,18]. To prepare the challenge agent, brains of terminally prion-sick mice infected with the Rocky Mountain Laboratories (RML) prion strain[45] were frozen, homogenized at 10% wt/vol in phosphate-buffered saline (Gibco 14190) using 1.4 mm zirconium oxide beads in 7 mL screw-cap tubes (CK14 soft tissue homogenizing kit, Precellys KT039611307.7) by means of 3x 40-second pulses on high in a Minilys homogenizer (Bertin EQ06404-200-RD000.0). 10% homogenate was then diluted 1:10 (vol/vol) to yield a 1% homogenate, irradiated with 7 kGy of X-rays on dry ice, extruded through finer and finer blunt-end needles (Sai infusion B18, B21, B24, B27, B30), and injected into sterile amber glass vials (MedLabSupply) and frozen. On the day of inoculation, vials were thawed and for each animal, 30 µL was drawn into a disposable insulin syringe with a 31 G 6 mm needle (BD SafetyGlide 328449). 7-week old C57BL/6N animals (Charles River) were placed under 3.0% isoflurane inhalation anesthesia, received meloxicam (5 mg/kg) for analgesia (one dose prophylactically and post-operative doses on following days), and heads were swabbed with povidone/iodine and alcohol swabs. The needle was then freehand inserted through the skull between the right ear and midline. After three seconds, the needle was withdrawn and animals were returned to home cages.

Animal monitoring

All animals undergoing ICV drug administration received post-operative monitoring daily for 4 days to surveil recovery and wound closure. In target engagement studies in non-prion animals, weights were generally collected prior to dosing and at 1-week intervals thereafter, although staffing constraints led to weights not being consistently collected in a subset of studies. Prion-infected animals had baseline body weights taken at 16 weeks of age (corresponding to 60 days-post inoculation, dpi) and weekly thereafter until 120 dpi, after which weights were taken thrice weekly. On the same monitoring schedule, we also collected behavioral scores and nest scores as described[18]. Behavioral scores were rated as 0 = absent, 1 = present for 8 symptoms: scruff / poor grooming, poor body condition, reduced activity, hunched posture, irregular gait/hindlimb weakness, tremor, blank stare, and difficulty righting. Nest scores were assigned for both cotton square nestlets (Ancare) and Enviro-dri® packed paper (Shepherd): 0 = unused; 1 = used/pulled apart, but flat; 2 = pulled into a three-dimensional structure; 0.5 and 1.5 were permitted intermediate scores. Animals were euthanized by CO2 inhalation (Euthanex) when

they reached -20% weight loss relative to individual baseline, or were deemed moribund, defined as unable to reach food or water. All monitoring was conducted, and endpoint decisions taken, by veterinary technicians blinded to treatment group (saline vs. non-targeting vs. active compound), although in studies with no injection controls, the lack of drug treatment in the control group could be inferred from the absence of surgery cards. As in our previous work, survival curves include deaths of all causes — animals are excluded only in cases of 1) death due to surgical complications on the day of surgery, 2) death prior to treatment group assignment, or 3) experimental error (for instance, wrong dose administered).

Tissue processing, PrP quantification, and RNA analysis

All quantification of PrP protein was performed on whole mouse brain hemispheres including cerebellum. Our in-house PrP ELISA has been previously described[46] and is summarized briefly as follows. Whole hemispheres were frozen on dry ice and later homogenized at 10% wt/vol in 0.2% CHAPS. The assay uses antibodies EP1802Y (Abcam, ab52604) for capture and in-house biotinylated 8H4 (Abcam ab61409) for detection, followed by streptavidin-HRP (Thermo Fisher Scientific, 21130) and TMB (Cell Signaling, 7004P4). Our calibrator curve from 5 ng/mL to 0.05 ng/mL utilized recombinant full-length mouse PrP (MoPrP23-231) expressed in *E. coli* and purified in-house[47]. We have previously shown[46] that this ELISA assay has indistinguishable reactivity for human and mouse PrP. Wild-type and Tg25109 brains were run at a 1:200 final dilution (10% homogenate diluted 1:20), while Tg26372 brains, because they overexpress PrP, were run at a 1:400 dilution. Each plate included high (WT), mid (het KO), and low (10% WT / 90% KO mix) brain homogenates used as QCs. To control against plate-to-plate variability, whenever one experiment produced more samples than could be run on one plate, we split every treatment group equally across 2 or more plates, and normalized each sample to the mean of the saline or no injection controls on its same plate. All results are expressed as residual PrP, a percentage of the control level. Across all experiments described here, the mid and low QCs usually read out at greater than the expected values of 50% and 10% residual PrP respectively, suggesting that the assay often overestimates residual PrP; for instance, the low QC, designed to mimic 10% residual PrP, averaged 17% residual PrP across all ELISA plates run in this study. Summary statistics on all ELISA plates are available in Figure S6. For RNA quantification, fresh brain hemispheres were placed in RNAlater (Sigma cat no: R0901) at 4°C before dissecting brain regions as described[46]. RT-qPCR was performed as described above using Taqman gene expression assays for mouse *Tbp* (Invitrogen, cat no: Hs00427620_m1) and human *PRNP* (Invitrogen, cat no: Hs00175591_m1) for transgenic mouse models or mouse Prnp (Invitrogen, cat no: Mm00448389_m1) for wild-type C57BL/6N mice.

Statistics, source code, and data availability

All analysis was conducted using custom scripts in R 4.2.0. Percent changes in mouse weights relative to baseline were compared using 2-sided T tests. Survival was assessed using log-rank

test. Dose-response curves were fit using the drc package[48] in R, fixing the infinite-dose asymptote (c) and zero-dose asymptote (d) at 0% and 100% respectively. The impact of scaffold and fixed tail was characterized using a linear model with formula residual ~ scaffold + log(dose) + region. Inflammatory marker responses were assessed using Dunnett's test to compare each treated group to the saline or untreated group. Raw individual-level animal data and source code sufficient to reproduce all analyses herein are available in this study's online git repository: https://github.com/ericminikel/divalent

Results

Divalent siRNA chemical scaffolds

We employed several distinct chemical scaffolds to test divalent siRNAs in vivo (Figure 1). The previously reported **s1** scaffold[29] and the **s2** variant with one additional 2′OMe modification each possess 7 phosphorothioate (PS) linkages at the 3′ end of the antisense (AS) strand (Figure 1). In the **s3** scaffold, the AS 3′ end is reduced to just 2 PS linkages, and in **s4**, these two 3′ nucleotides are further stabilized with the extended nucleic acid (exNA) modification[33].

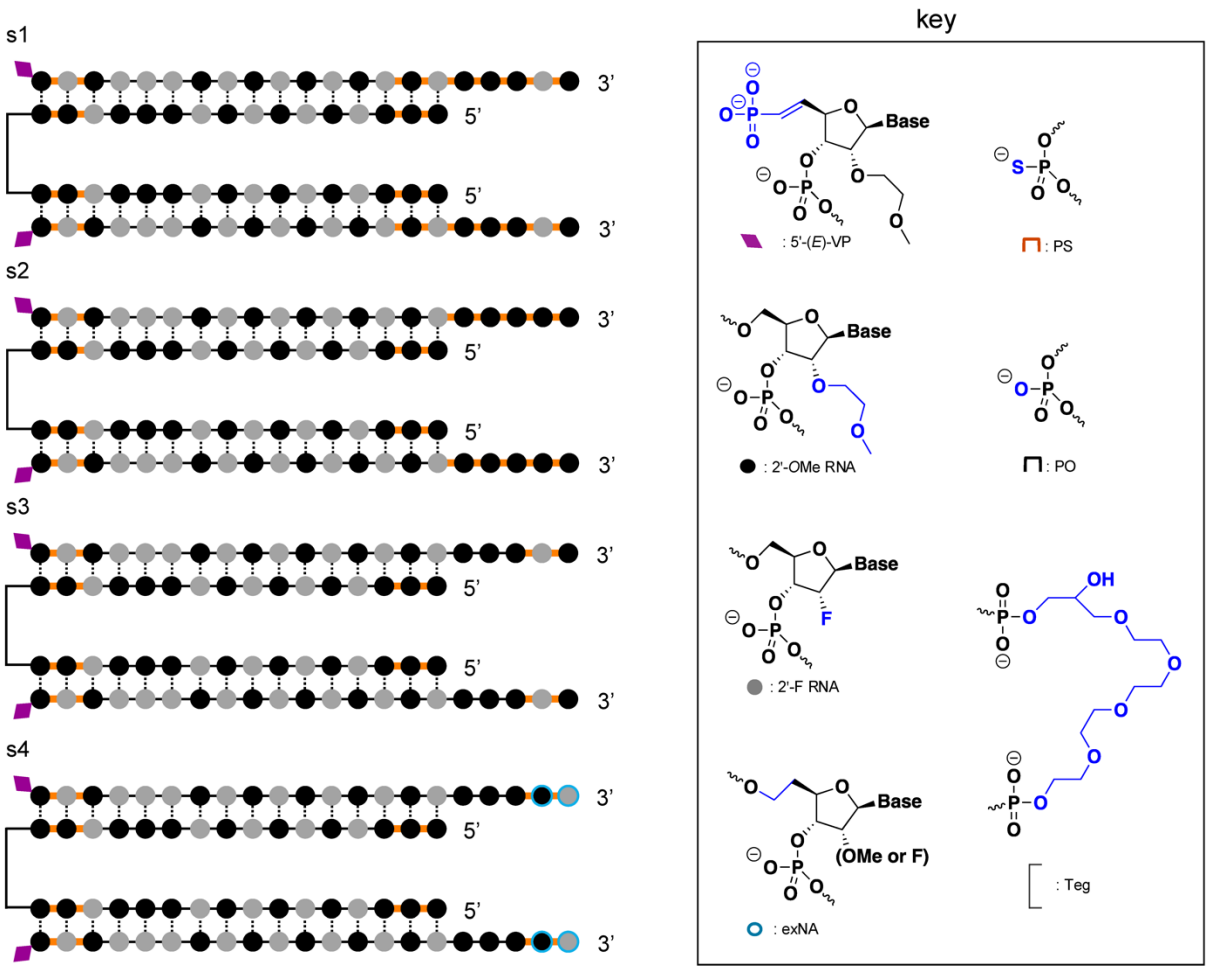

Figure 1. Chemical scaffolds used in this study. *Abbreviations: 5'-(E)-VP, 5'-vinyl phosphonate; 2'-OMe, 2'-O-methyl; 2'-F, 2'-fluoro; exNA, extended nucleic acid; PS: phosphorothioate; PO: phosphodiester; Teg: tetraethylene glycol. Additional scaffolds that feature only in supplementary figures are shown in Figure S1.*

Proof of concept in a prion disease model

We screened 20 siRNA sequences (Table S1) against mouse *Prnp* in mouse N2a cells, advancing 4 sequences into dose-response[49] (Figure S2). These studies nominated sequence 1682 as a tool compound for mouse *Prnp*; we also considered sequence 1035 due to its activity in human A549 cells (Figure S2) and its predicted cross-reactivity to mouse. Screening additional compounds in N2a cells by qPCR (Figure S3) yielded no additional strong hits. We tested 1682 and 1035 in wild-type C57BL/6N mice using a bilateral ICV bolus dose totaling 348 µg with tissue collection at 3-4 weeks post-dose and whole brain hemisphere total PrP quantified by ELISA[46] as a primary endpoint (Figure 2A). 1035 exhibited weak activity, with 81.8% residual PrP in the s1 scaffold (1035-s1), which improved with the s4 scaffold reaching 64.1% residual PrP. 1682-s4 was the most potent with 49.4% residual PrP, similar to previously reported ASO tool compounds[18,46].

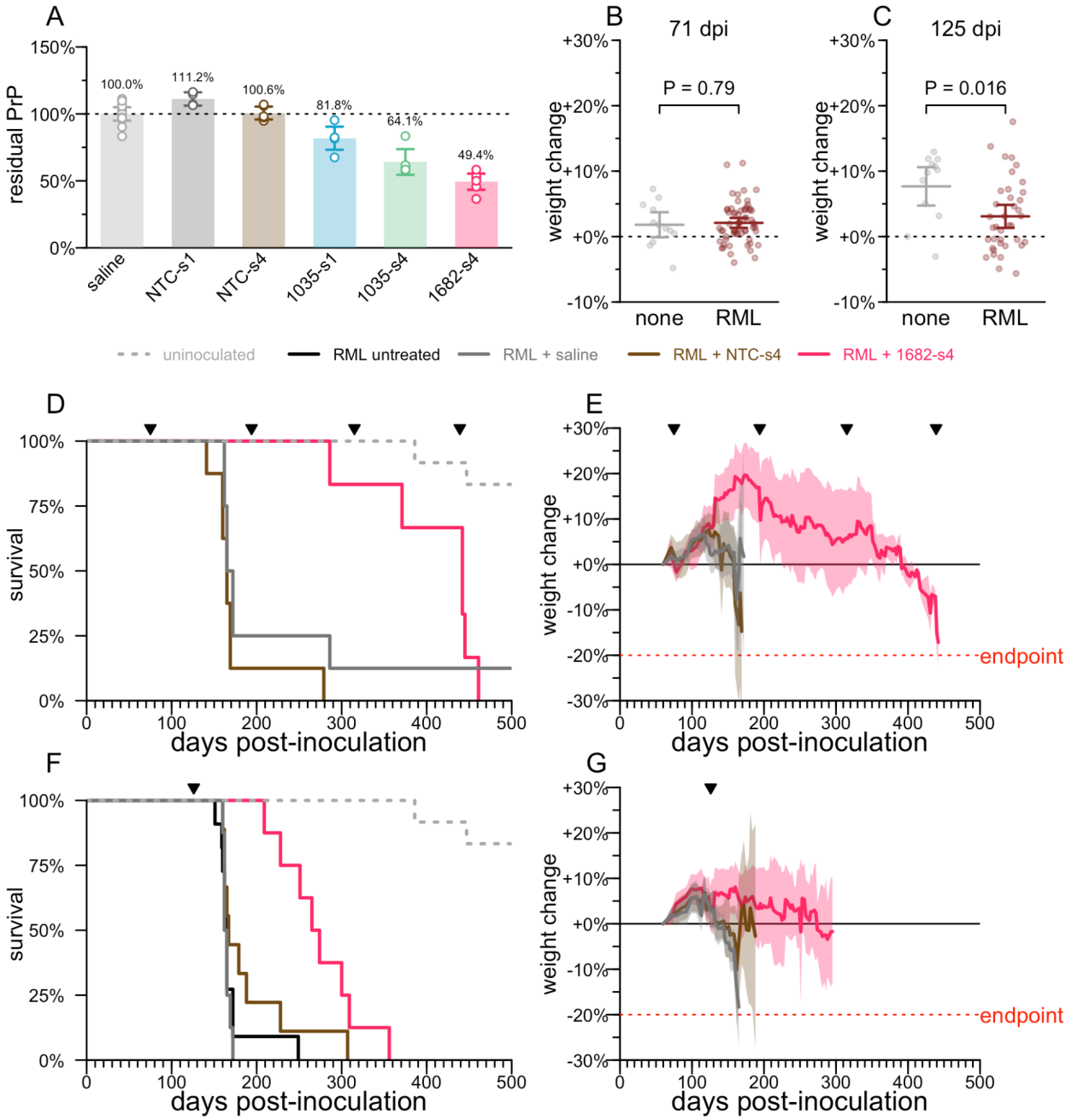

Figure 2. PrP lowering by divalent siRNA is effective in a mouse model of prion disease. ***A)*** *Whole brain hemisphere PrP quantified by ELISA from 3-4 week target engagement studies in wild-type mice receiving 348 µg of divalent siRNA or saline.* ***B)*** *Weight change relative to individual animal baseline in animals at 71 dpi, the last timepoint at which they were weighed prior to the 75 dpi intervention. At this timepoint, animals are asymptomatic and there is no difference in body weights (2-sided T test) between animals inoculated with RML prions (RML) or uninoculated (none).* ***C)*** *Weight change relative to individual animal baseline in animals at 125 dpi, the last timepoint at which they were weighed prior to the 126 dpi intervention; this plot*

excludes animals treated beginning at 75 dpi. At this timepoint, animals are symptomatic, as evidenced by a significant difference in body weights (2-sided T test). ***D)*** *Survival of animals in the early (75 dpi) intervention group. Saline N=7, NTC-s4 N=8, 1682-s4 N=6, uninoculated N=12. Ticks at the top show the dates of ICV drug administration.* ***E)*** *Weight trajectories of animals in the early (75 dpi) intervention group, expressed as percent change from each animal's individual baseline. Solid lines are means, shaded areas are 95% confidence intervals.* ***F)*** *As in (D) but for the late (126 dpi) intervention group. No treatment N=11, saline N=8, NTC-s4 N=9, 1682-s4 N=8. The same group of uninoculated N=12 from (D) is repeated here for reference.* ***G)*** *As in (E) but for the late (126 dpi) intervention group.*

We intracerebrally inoculated wild-type mice with the RML strain of prions[45], which yields neuropathological changes detectable at the molecular level by ~60 dpi but no symptoms until at least 120 dpi[18]. At 71 dpi, there was no difference in individual weight gain trajectory between inoculated mice and uninoculated controls, consistent with the presymptomatic disease stage (Figure 2B). In contrast, by 125 dpi, weight gain was significantly attenuated in the inoculated compared to uninoculated mice (P = 0.016), indicative of a symptomatic disease stage (Figure 2C).

Chronic dosing of 348 µg of 1682-exNA every 120 days (q120d) beginning at a presymptomatic timepoint of 75 dpi caused treated animals to significantly outlive controls by 2.7-fold (median 442 vs. 165 dpi, P = 0.0002, log-rank test, Figure 2D), with disease-attendant weight loss both delayed and slowed (Figure 2E). A single 348 µg dose given at a symptomatic timepoint of 126 dpi yielded survival time 3.5 months longer than controls (median 270 vs. 164 dpi, P = 0.0002, log-rank test, Figure 2F), with further weight loss delayed and slowed (Figure 2G). This difference amounts to a 64% increase in total survival time, or a 3.8x increase in remaining survival time from the moment of treatment at 126 dpi. All animals eventually succumbed to typical prion disease symptoms and the majority met the pre-specified weight loss endpoint. Non-targeting control (NTC) divalent siRNAs, which did not lower PrP (Figure 2A), also did not increase survival time (Figure 2D, 2F), confirming on-target lowering of PrP as the mechanism of action.

These experiments confirmed that PrP lowering by divalent siRNA is effective against prion disease.

Generation of human *PRNP* transgenic mice

The observation of efficacy of PrP lowering by targeting the PrP RNA with divalent siRNA above led us to seek potent divalent siRNA compounds targeting the human *PRNP* gene. In vivo potency testing of siRNA sequences for human drug candidates requires transgenic mice expressing the full human *PRNP* gene including non-coding sequence.

We generated two new BAC transgenic lines harboring the full human *PRNP* gene, crossed them to homozygosity for endogenous *Prnp* knockout (ZH3/ZH3)[38], and determined their

transgene integration sites, copy numbers, and human PrP expression level (Table 1, Figure 3). Tg25109 heterozygotes, with just 3 transgene copies, expressed human PrP at levels barely above wild-type (Figure 3A), while Tg26372 homozygotes, with 20 transgene copies, expressed human PrP at 5.4x the wild-type level (Figure 3A). The relationship between transgene DNA copy number and protein expression was sub-linear, just as observed[13] for transgenes encoding mouse PrP (Figure 3B). Short-read sequencing of the Tg26372 mouse confirmed integration of 46.0kb of human sequence from the major and ancestral 129M haplotype: 20.5 kb upstream, 15.2 kb spanning from the *PRNP* transcription start to stop site, and 10.3kb of downstream sequence (Figure 3C). The transgene excludes the downstream gene *PRND*, for which overexpression in the brain is known to be toxic.

Table 1. Transgenic human PRNP mice. *Each line harbors a tandem array of the same 46.0 kb bacterial artificial chromosome (BAC) containing human PRNP 129M, randomly integrated into a different site in the mouse genome, see Methods for details. All mice are on a C57BL/6N background and PrP expression level was determined relative to WT C57BL/6N mice, n=3-6 per group. *Tg25109 homozygotes were subviable, see Results for details.*

Line	Integration site	Genes disrupted at integration site	Het copy number	Het PrP expression	Hom copy number	Hom PrP expression
Tg25109	chr12	*Frdm6*, *Tmx1*	3	1.1	6*	2.0*
Tg26372	chr18	*Dok6*	10	3.4	20	5.4

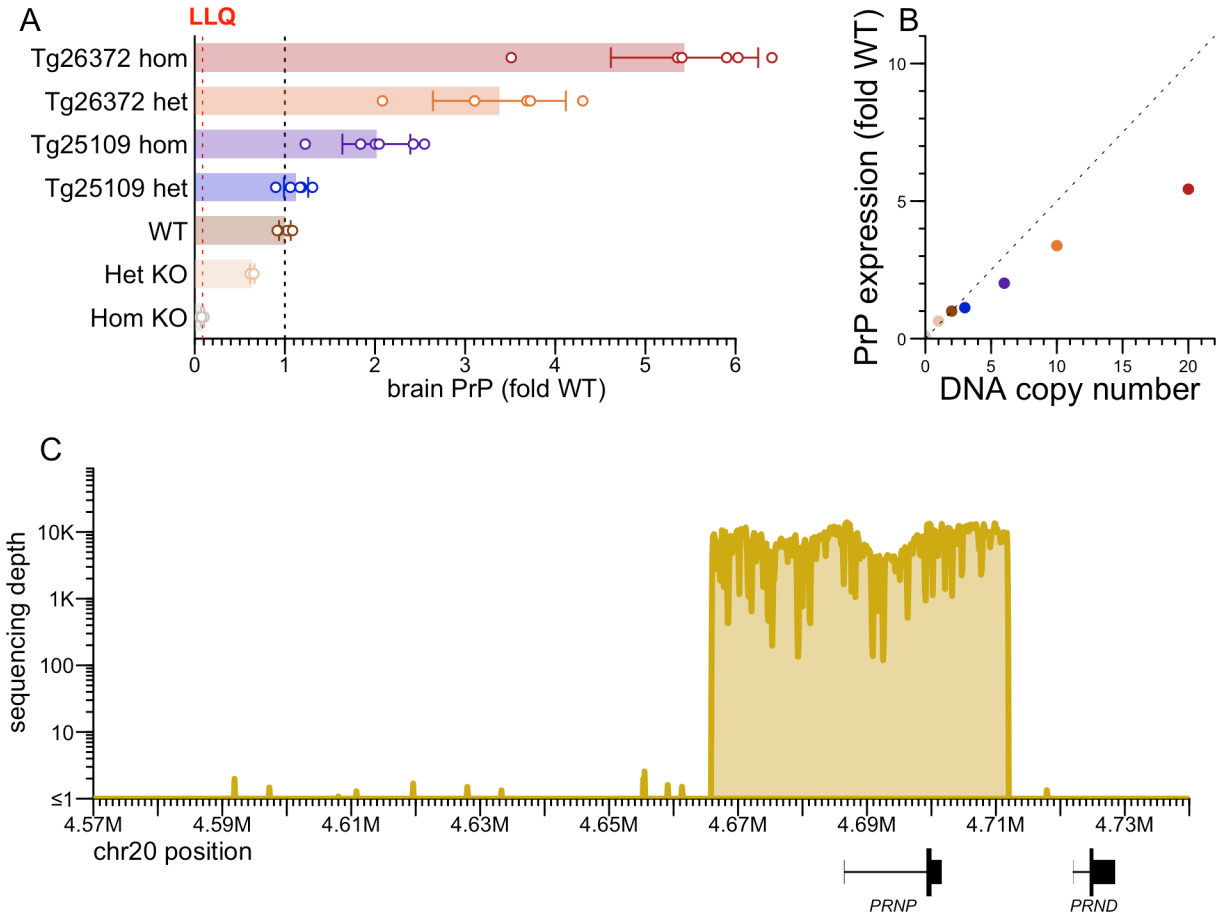

Figure 3. Characterization of human PRNP BAC transgenic mice. A) *PrP concentration in whole brain hemispheres, normalized to the mean of wild-type (WT) animals. Points are individual animals. N=3-6 per group. Rectangular bars are means. Error bars are 95% confidence intervals.* ***B)*** *PrP expression from (A) versus gene copy number at the DNA level; the dashed line with slope 0.5 represents the linear relationship whereby 2 gene copies = 1x expression.* ***C)*** *Extent of human sequence in the BAC, based on targeted capture sequencing (Methods) with reads aligned to the human genome reference (GRCh38), using genomic DNA from a Tg26372 mouse.*

Heterozygote-heterozygote crosses of our Tg25109 (3x) line yielded a ratio of 98:198:32 (non-transgenic:heterozygote:homozygote), a significant deviation from Mendelian ratio ($P < 1e\text{-}15$, Chi-square test). Of 4 Tg25109 homozygous x homozygous pairs mated, only 1 pup was ever born. We examined the literature evidence for viability of knockouts for *Tmx1* and *Frmd6*, the two genes disrupted at the Tg25109 integration site (Table 1). *Tmx1* (formerly known as *Txndc1*) homozygous knockout mice were reported to have abnormal bone metabolism and immunology[50], while *Frdm6* homozygous knockout mice were reported to have several phenotypes including eye and hematological defects and were born at less than the expected Mendelian ratio from het-het crosses[51,52] (41:51:15, $P = 0.0016$, Chi-square test). The sub-viability of Tg25109 homozygous mice therefore likely arises from knockout of *Frdm6,* or from

the combination of both *Frmd6* and *Tmx1*. It is unlikely to be transgene expression-related, as Tg26372 homozygous mice, with higher copy number (20 vs. 6) and protein expression (5.4 vs. 2.0x wild-type) were unaffected. Given the difficulty of obtaining adequate numbers of Tg25109 homozygotes for experiments, we excluded this genotype from further experiments. Given the convenience of maintaining Tg26372 as obligate homozygotes, we performed the vast majority of experiments in this genotype, but 2 compounds also tested in Tg25109 heterozygotes showed target engagement in both genotypes (Figure S5).

These mice provided us a model in which to develop siRNA compounds against the human *PRNP* RNA.

Identification of compounds targeting human *PRNP*

A screen of 24 predicted active compounds in human A549 cells identified 4 hits with dose-responsive potency, led by sequence 2440 (Figure S2)[49]. We conducted an expanded screen of 84 compounds in human U251-MG glioblastoma cells, prioritizing predicted hot spots within a ±3 base pair walk of the top sequences from the initial screen (Figure 4A). At a 2.0 μM screening concentration, 34 compounds (40%) yielded <10% residual *PRNP*. The 0.5 μM screening concentration provided better power to discriminate the most potent sequences, with just 14 (17%) yielding <10% residual *PRNP* (Figure 4A). 10 sequences tested in dose-response all proved active with IC_{50} < 100 nM (Figure 4B).

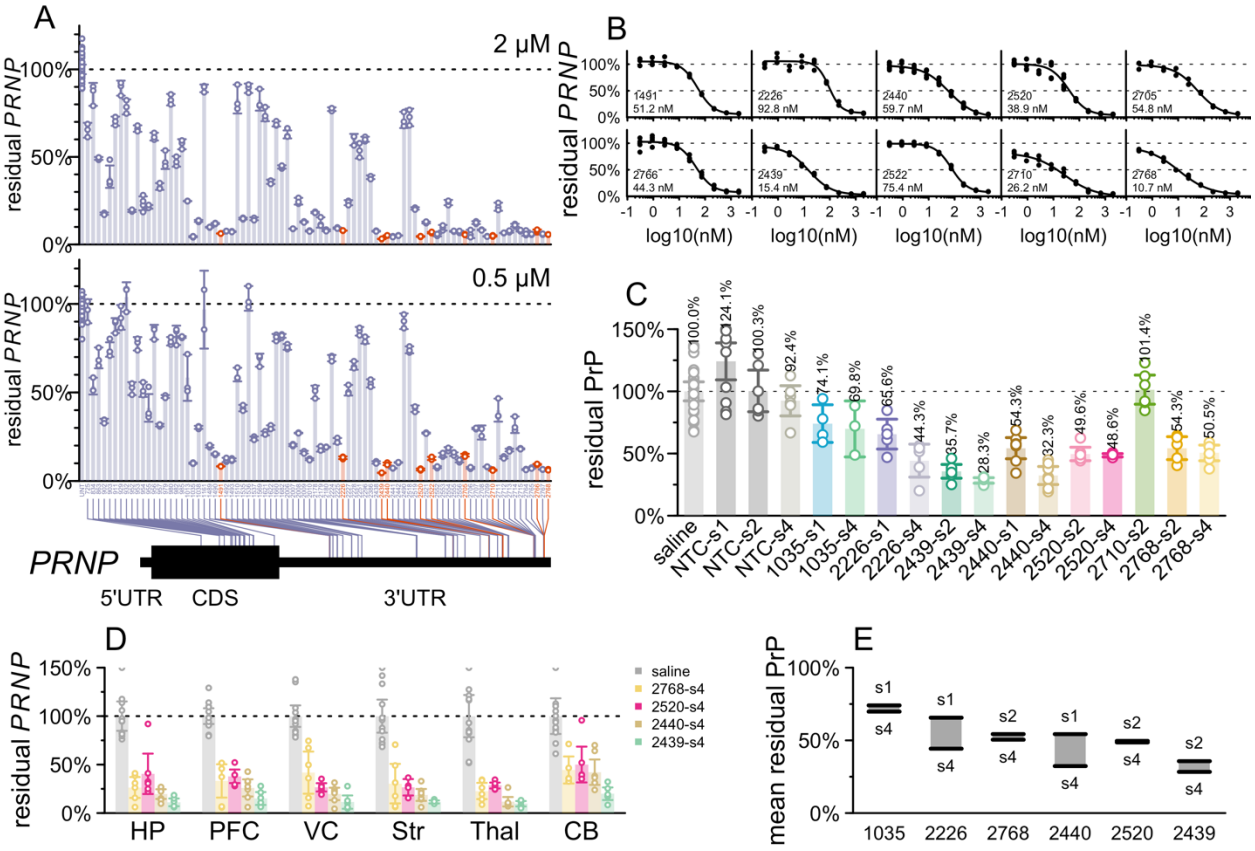

Figure 4. Identification of human PRNP-targeting siRNA sequences. A) *In cellulo screening using scaffold Chol-TEG s2 (Figure S1). The readout is PRNP qPCR, normalized to the mean of untreated (UNT) controls. Each point represents 1 well of U251-MG human glioblastoma cells, run in qPCR technical duplicate. Rectangular bars represent the mean of triplicate wells, and error bars represent the 95% confidence intervals. Screening used Chol-Teg conjugated monovalent siRNAs (Figure S1) by gymnotic uptake at 2.0 μM (top panel) or 0.5 μM (bottom).* ***B)*** *Dose-response testing in cell culture. The readout is PRNP qPCR. Points represent individual wells of U251-MG cells, curves are four-parameter dose-response curves fit by the drc package in R. Displayed at bottom are the sequence number and the calculated IC_{50} value.* ***C)*** *In vivo testing. The readout is PrP ELISA. Each point represents a whole brain hemisphere of one Tg26372 homozygous mouse, rectangular bars represent the group mean, and error bars represent the 95% confidence intervals. N=3-7 per group, total 120 animals.* ***D)*** *Regional PRNP qPCR for select compounds from the same animals in panel (C), in mouse hippocampus (HP), prefrontal cortex (PFC), visual cortex (VC), striatum (Str), thalamus (Thal), and cerebellum (CB).* ***E)*** *Data replotted from panel (C) — difference between mean residual PrP for the s1/s2 (high PS, no exNA) scaffolds versus the s4 (reduced PS, with exNA) scaffold for 6 sequences where both were tested in vivo.*

7 sequences selected based on potency as well as cross-reactivity were advanced to in vivo screening in multiple chemical scaffolds (Figure 1, Figue 4C) alongside saline and NTC controls, for a total of 17 experimental groups totaling 120 Tg26372 homozygous animals. Each compound was tested at a 348 μg dose, with whole brain hemispheres collected at 4-5 weeks

post-dose analyzed by ELISA. Non-targeting controls did not significantly lower PrP in any chemical configuration tested. In either chemical scaffold, 2439 proved to be the most potent sequence in vivo (Figure 4C). RT-qPCR analysis for the top 4 sequences tested in the s4 scaffold confirmed that 2439 achieved deeper *PRNP* RNA lowering than the other 3 sequences in 6/6 mouse brain regions tested (Figure 4D). For all compounds, lowering was weakest in the cerebellum, as reported for a divalent siRNA targeting *HTT*[28], likely due to lower drug accumulation in rodent cerebellum. The deeper lowering at the RNA level (residual ranging from 9.6% in thalamus to 19.9% in cerebellum) than at the protein level (28.3% residual in whole hemisphere) in this experiment may simply reflect floor effects in our ELISA: a contrived sample designed to mimic 10% residual PrP (10% wild-type brain homogenate mixed with 90% knockout brain homogenate) read out as an average of 17% of wild-type across all ELISA plates in this study (Figure S6). For 6/6 sequences where both a high-phosphorothioate (s1 or s2) and the low-phosphorothioate plus exNA s4 scaffold were tested, s4 proved the more potent, by a margin of 1 to 21 percentage points of PrP lowering (Figure 4E), as shown for *Htt* and *Apoe*[33].

We used tribromoethanol as an anesthetic for our initial studies because it was used for divalent siRNA previously[28]. We later pivoted to 3% isoflurane anesthesia with incorporation of divalent cations (a 14:2:1 molar ratio of Ca^{2+}:Mg^{2+}:divalent siRNA) into the injectable solution, which has been reported to eliminate seizures upon injection of high-dose oligonucleotides into CSF[41]. All animals recovered from anesthesia normally, we never observed seizures. Animals generally gained weight for the duration of the in-life period (Figure S5), with the exception of compound 2520-s2, for which 5/6 animals experienced acute weight loss between 3 and 4 weeks post-dose. To further assess tolerability, performed RT-qPCR for neuroinflammatory markers *Gfap* and *Iba1* in the visual cortex. None of the sequences tested significantly affected *Gfap* (all $P > 0.10$, Dunnett's test); only 2520-s4 marginally impacted *Iba1* (43% decrease, P = 0.046, Dunnett's test; Figure S5). 2439 exhibited a favorable in silico predicted off-target profile: antisense strand bases 2-17 harbored at least 2 mismatches to all human protein-coding mRNAs other than *PRNP* (Supplementary Tables).

These studies nominated 2439 as our lead sequence.

Comparison of chemical scaffolds and antisense strand 3′ tails

The in cellulo and in vivo screening results nominated 2439 as the lead sequence (Figure 4C) and provided some evidence that the s4 scaffold was superior to the s1 and s2 scaffolds (Figure 4E), but we sought additional evidence to confirm the lead scaffold before proceeding. Our s4 compounds were all synthesized with a fixed 3′-UU tail mismatched to the target RNA, initially due to the relative ease of synthesis of mxU and fxU phosphoramidites[33] and the unavailability of their A, G, or C equivalents. In contrast, our s1 and s2 compounds were synthesized with full complementarity to the target RNA. Depending upon sequence, unmatched 3′ tails can facilitate PAZ binding[53] without compromising RISC activity[54,55]. Complete complementarity has even been associated with increased rates of RISC unloading[34] and target-directed degradation[35].

We therefore sought to determine for the lead sequence the relative contributions of the PS and exNA modifications that distinguish the s4 scaffold, versus the effect of this 3′ fixed tail.

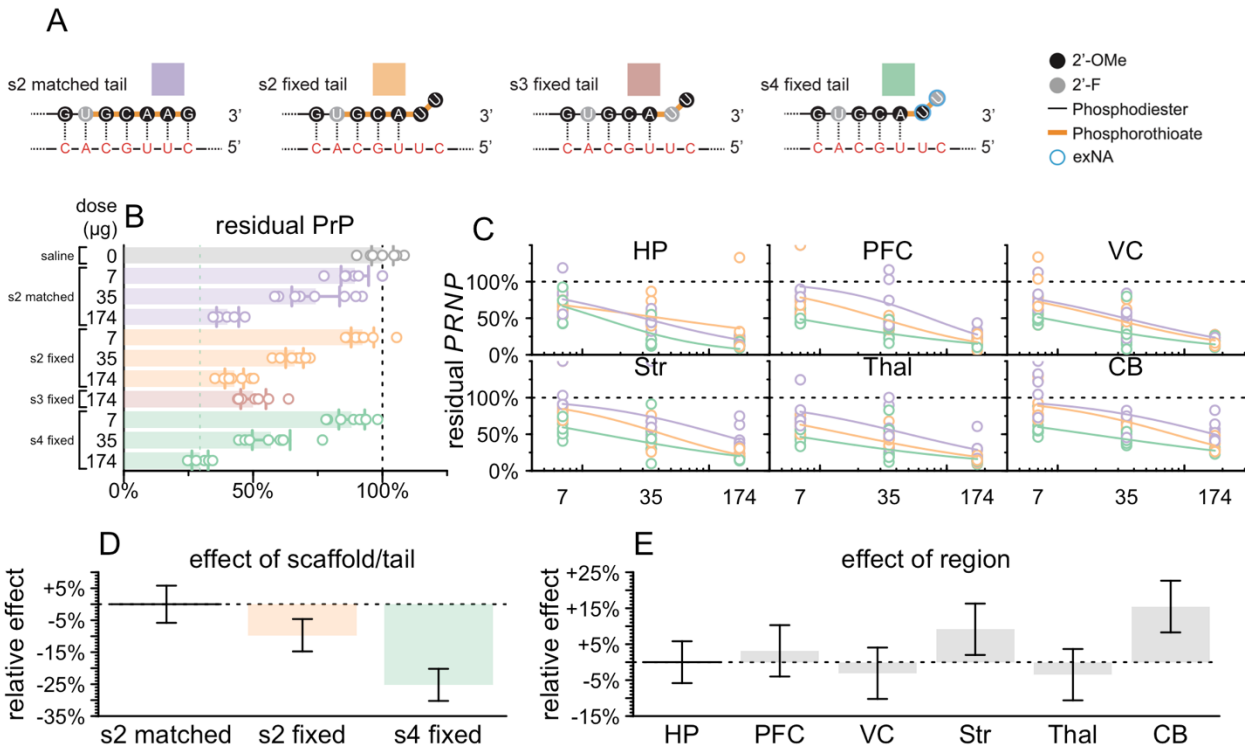

Figure 5. Impact of chemical scaffold and 3' antisense tail on lead sequence potency. A) *Color key and diagram of differences between 4 compounds tested. These compounds differ only in the 3' tail of the antisense strand shown here. The antisense strand of the divalent siRNA is shown at top, and the target mRNA is shown in red below. Each compound was injected at the doses indicated in B-C into N=8 animals harvested after 30 days.* ***B)*** *Whole hemisphere residual PrP by ELISA (x axis) by compound and dose (y axis). Each point is one animal, rectangular bars are means, error bars are 95% confidence intervals.* ***C)*** *Regional PRNP RNA by qPCR (y axis) versus dose (x axis). Each point is one animal. Curves are 4-parameter log-logistic dose-response curves (see Methods).* ***D)*** *Linear model coefficients for scaffolds fit to the data in (C).* ***E)*** *Linear model coefficients for brain regions fit to the data in (C).*

We performed a 3-point in vivo dose response experiment with 5-fold dose increments (7, 35, and 174 µg) for each of 3 scaffolds (s2 matched tail, s2 fixed tail, s4 fixed tail) versus saline controls, N=8 per group, with harvest at 4 weeks. We also included s3 fixed tail at only the highest dose (174 µg) to test our assumption that reduction of PS content without introduction of exNA would result in reduced activity.

At every dose level, 2439-s4 was the superior compound in terms of whole-hemisphere PrP, with 29.5% residual at the 174 µg dose (Figure 5A). As expected, the s3 scaffold with fixed tail performed more poorly than any other scaffold at the high dose (Figure 5A). We performed RT-qPCR for *PRNP* RNA and fit dose-response curves for 6 brain regions (Figure 5C), and used a

linear model (Methods) to characterize the effects of scaffold/tail combination, brain region, and dose level. This model indicated that s1 fixed tail provided 9.4 percentage points deeper *PRNP* lowering than s1 matched tail (P = 0.0017), while the s4 fixed tail conferred another 15.9 percentage points beyond s1 fixed tail (P = 5.0e-11, Figure 5D). Thus, both the fixed tail and the terminal exNA modification contributed to the potency of the s4 scaffold. At the middle dose (35 µg), 2439-s4 yielded <50% residual *PRNP* in 6/6 brain regions tested (Figure 5C), with target engagement weakest in cerebellum (Figure 5E) as expected[28]. Individual dose-response curves for each scaffold/tail combination in each brain region yielded median effective dose (ED_{50}) for 2439-s4 ranging from 5 µg in thalamus to 18 µg in cerebellum.

This experiment confirmed 2439-s4 with its fixed 3′-UU tail (full structure in Figure S7) as our drug candidate.

Durability and dosing regimens for drug candidate

We tested the durability of effect of 2439-s4 in 2 studies. After a 348 µg dose we observed 17% and 40% residual PrP in whole hemispheres at 34 and 120 days post-dose (Figure 6A). After a 174 µg dose we observed 29%, 51%, and 74% residual PrP at 29, 91, and 180 days post-dose (Figure 6B). The same sequence in 2 scaffolds with higher PS content provided superior durability but lower initial knockdown at the 1-month timepoint (Figure S8).

We also explored the effect of a loading dose administered 7 days after the initial dose, and of repeat dosing after 90 days (Figure 6C). When the 348 µg dose was given at day 0, 7, and 90, the residual PrP in whole hemisphere at day 120 was 15%. We also evaluated a 52 µg dose which may more realistically correspond to dose levels reachable clinically (see Discussion). Compared to a single dose at day 0, a loading dose regimen (day 0 and 7) for 52 µg provided improved target engagement at day 30 (32% vs. 49% residual PrP), with 5/6 regions below 25% residual *PRNP* RNA (Figure S9A); all regions were below the respective levels reached with the 348 µg dose of 1682-s2 (Figure S9B) in the survival study (Figure 2). An additional dose at day 90 yielded 41% residual at day 120.

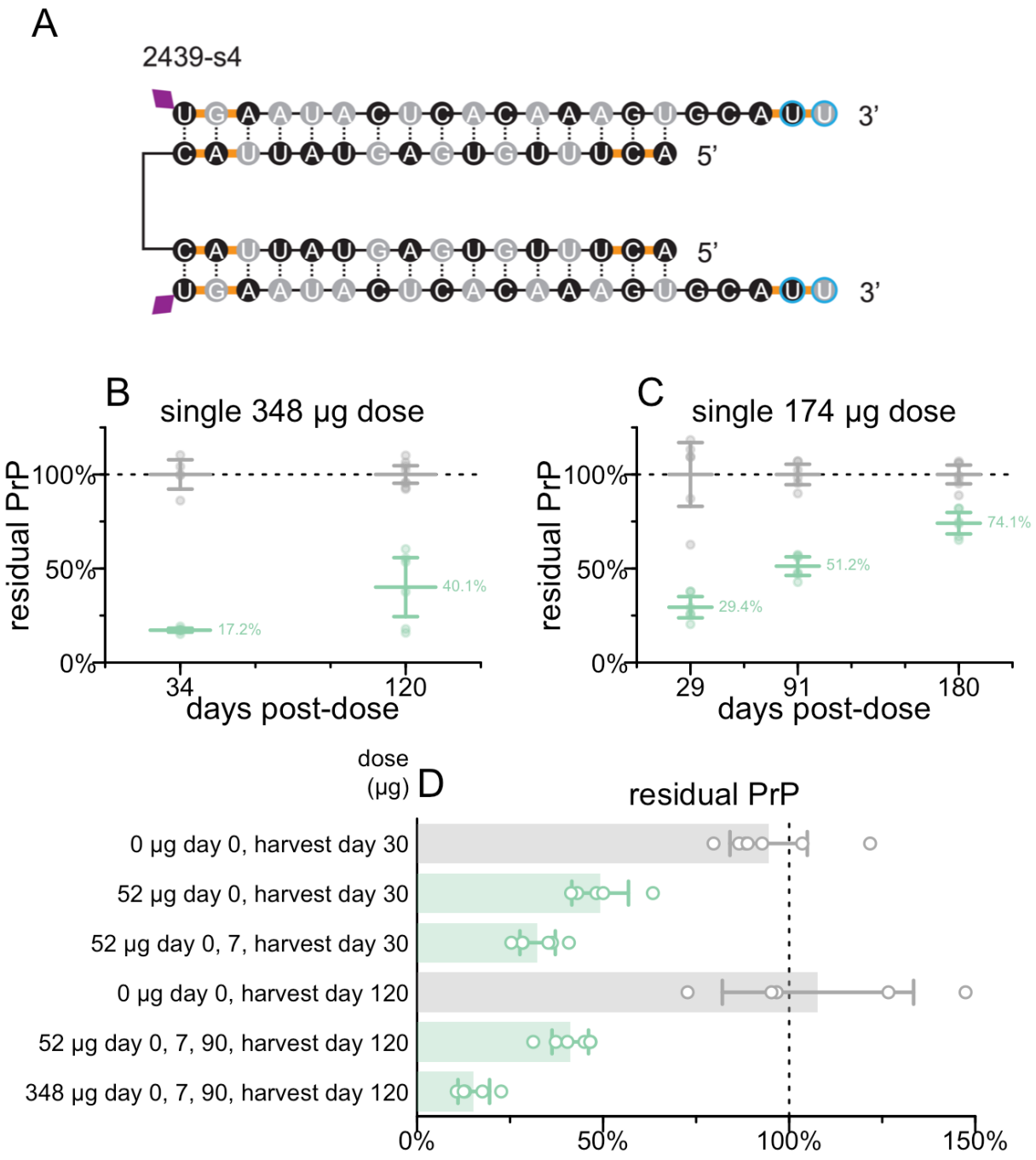

Figure 6. Characterization of lead compound 2439-s4. A) *Identity of 2439-s4.* ***B)*** *Durability of effect of a single 348 µg dose in Tg26372 animals. Whole hemisphere PrP (y axis) versus months post-dose (x axis). Each point is one animal, horizontal line segments are means, error bars are 95% confidence intervals.* ***C)*** *Durability of effect of a single 174 µg dose in Tg26372 animals. Whole hemisphere PrP (y axis) versus months post-dose (x axis). Each point is one animal, horizontal line segments are means, error bars are 95% confidence intervals.* ***D)*** *Impact of repeat dosing regimens on target engagement in Tg26372 animals. Whole hemisphere PrP*

(x axis) for indicated dose levels and regimens (y axis). Each point is one animal, rectangular bars are means, error bars are 95% confidence intervals.

These experiments indicated that a single dose of divalent siRNA can provide target engagement and durability expected to be meaningful on the time course of prion disease, while repeat dosing further improves target engagement.

Discussion

We nominate PrP-lowering divalent siRNA 2439-s4 as a new drug candidate for treating prion disease. Our study shows that lowering PrP RNA with this modality is effective against prion disease, and that the human drug candidate is potent, long-lasting, and appears well-tolerated.

As with ASOs[17,18], we observed an extension of healthy life in prion-infected animals treated pre-symptomatically with divalent siRNA, whereas in already-symptomatic animals treatment extended life without reversing existing weight loss. This is consistent with an inability of PrP lowering to address pre-existing neuronal loss, and with a lag time of a few weeks between target engagement at the RNA level and maximal lowering of PrP at the protein level[44]. Our data support treatment of prion disease patients at both symptomatic and pre-symptomatic timepoints, while suggesting that the greatest good can be achieved in a pre-symptomatic preventive paradigm[2].

The drug candidate 2439-s4 appears to have favorable properties in terms of potency and durability. We observed a depth of target suppression — as low as 17% residual whole hemisphere PrP after a single 348 µg dose and 15% with repeat dosing — never previously reported for PrP, and we showed at least some activity out to 6 months after a single dose. The ED_{50} for the candidate in mice, measured by regional qPCR, ranges from 5 - 18 µg depending upon brain region, which compares favorably to the ED_{50} values ranging from 27 µg (in spinal cord) to 69 µg (in cortex) reported for the most potent human ASO candidate against PrP[56]. Using CSF volume scaling (0.04 mL in mice versus 130 mL in human[57,58], a factor of 3,250),18 µg might correspond to 58 mg in a human. This dose level is clinically precedented for oligonucleotides — the ASO tofersen for *SOD1* ALS is dosed at 100 mg[59]. These calculations lead us to hypothesize that a single dose of 2439-s4 could lower PrP by 50% in many human brain regions, which is important because prion disease is a whole brain disease. A limitation of our study, however, is that uniformity of brain exposure is a major challenge for any intrathecally delivered oligonucleotide therapy, and we did not assess biodistribution and target engagement in a pharmacodynamically relevant large animal species. Divalent siRNAs dosed into non-human primates or sheep by ICV or IT routes[28,60,61] were reported to have broad distribution and activity, although, as with ASOs[62], deep subcortical brain regions are less well-reached, with drug concentration in putamen being <20% that achieved in cortex.

Another limitation of our study is that, although we demonstrated efficacy in a disease model using a tool compound, we did not assess the disease modifying impact of the deeper PrP lowering achieved with our clinical candidate. Recent reports of researchers dying of prion

disease after occupational exposure to human prion-infected brain tissue[63,64] convinced us to not examine the efficacy of our drug candidate in a challenge study with human prions in our humanized mice. Our drug candidate is not cross-reactive for mouse *Prnp*, precluding rescue studies in wild-type mice. Thus, we were unable to measure the survival benefit attainable by the deeper PrP lowering observed with our drug candidate compared to our mouse *Prnp* tool compound. Delay of prion disease by PrP lowering is dose-responsive[18], and homozygous knockouts are invulnerable to prions[10], anchoring our assumption that deeper lowering is better. Nevertheless, at present we lack an animal model system to answer in a more quantitative way what benefit will be achieved by the deep PrP lowering described here — for instance, whether prion replication or symptom progression could be halted.

The major outcome of our studies is to nominate PrP-lowering divalent siRNA 2439-s4 as a novel drug candidate for prion disease.

Acknowledgments

This study was funded by the National Institutes of Health through Innovation Grants to Nurture Initial Translational Efforts (IGNITE R61/R33 NS119717) and the Ultra-rare Gene-based Therapy Network (URGenT U01 NS132994), and by Prion Alliance and Brokaw Family Foundation.

Competing interest statement

AK is a co-founder, scientific advisory board member, and shareholder of Atalanta Therapeutics, as well as a founder of Comanche Pharmaceuticals and on the scientific advisory board of Aldena Therapeutics, AlltRNA, Prime Medicine, and EVOX Therapeutics. AK, JA, and MRH are co-inventors on patents WO2016161388 and WO2017132669 relating to background technology for divalent siRNA. AK and KY are co-inventors on patents WO2020198509, WO2021195533, and WO2021242883 relating to the exNA nucleotide modification. AK and ZK are co-inventors on patent WO2021173984, and JEG, ZK, KY, EVM, AK, and SMV are co-inventors on U.S. provisional patent application 63/564,255 filed by UMass Chan Medical School, relating to divalent siRNA for prion disease. CLGB, MRH, GK, and ALJ are employees and shareholders of Atalanta Therapeutics. JA and DC are former employees of Atalanta Therapeutics, and DC is a shareholder. EVM acknowledges speaking fees from Abbvie, Eli Lilly, and Vertex; consulting fees from Alnylam and Deerfield; research support from Eli Lilly, Gate Bio, Ionis, and Sangamo. SMV acknowledges speaking fees from Abbvie, Biogen, Eli Lilly, Illumina, and Ultragenyx; consulting fees from Alnylam and Invitae; research support from Eli Lilly, Gate Bio, Ionis, and Sangamo.

References

1. Prusiner SB. Prions. Proc Natl Acad Sci U S A. 1998 Nov 10;95(23):13363–13383. PMCID: PMC33918

2. Vallabh SM, Minikel EV, Schreiber SL, Lander ES. Towards a treatment for genetic prion disease: trials and biomarkers. Lancet Neurol. 2020 Apr;19(4):361–368. PMID: 32199098

3. Büeler H, Fischer M, Lang Y, Bluethmann H, Lipp HP, DeArmond SJ, Prusiner SB, Aguet M, Weissmann C. Normal development and behaviour of mice lacking the neuronal cell-surface PrP protein. Nature. 1992 Apr 16;356(6370):577–582. PMID: 1373228

4. Richt JA, Kasinathan P, Hamir AN, Castilla J, Sathiyaseelan T, Vargas F, Sathiyaseelan J, Wu H, Matsushita H, Koster J, Kato S, Ishida I, Soto C, Robl JM, Kuroiwa Y. Production of cattle lacking prion protein. Nat Biotechnol. 2007 Jan;25(1):132–138. PMCID: PMC2813193

5. Yu G, Chen J, Xu Y, Zhu C, Yu H, Liu S, Sha H, Chen J, Xu X, Wu Y, Zhang A, Ma J, Cheng G. Generation of goats lacking prion protein. Mol Reprod Dev. 2009 Jan;76(1):3. PMID: 18951376

6. Bremer J, Baumann F, Tiberi C, Wessig C, Fischer H, Schwarz P, Steele AD, Toyka KV, Nave KA, Weis J, Aguzzi A. Axonal prion protein is required for peripheral myelin maintenance. Nat Neurosci. 2010 Mar;13(3):310–318. PMID: 20098419

7. Benestad SL, Austbø L, Tranulis MA, Espenes A, Olsaker I. Healthy goats naturally devoid of prion protein. Vet Res. 2012;43:87. PMCID: PMC3542104

8. Minikel EV, Vallabh SM, Lek M, Estrada K, Samocha KE, Sathirapongsasuti JF, McLean CY, Tung JY, Yu LPC, Gambetti P, Blevins J, Zhang S, Cohen Y, Chen W, Yamada M, Hamaguchi T, Sanjo N, Mizusawa H, Nakamura Y, Kitamoto T, Collins SJ, Boyd A, Will RG, Knight R, Ponto C, Zerr I, Kraus TFJ, Eigenbrod S, Giese A, Calero M, de Pedro-Cuesta J, Haïk S, Laplanche JL, Bouaziz-Amar E, Brandel JP, Capellari S, Parchi P, Poleggi A, Ladogana A, O'Donnell-Luria AH, Karczewski KJ, Marshall JL, Boehnke M, Laakso M, Mohlke KL, Kähler A, Chambert K, McCarroll S, Sullivan PF, Hultman CM, Purcell SM, Sklar P, van der Lee SJ, Rozemuller A, Jansen C, Hofman A, Kraaij R, van Rooij JGJ, Ikram MA, Uitterlinden AG, van Duijn CM, Exome Aggregation Consortium (ExAC), Daly MJ, MacArthur DG. Quantifying prion disease penetrance using large population control cohorts. Sci Transl Med. 2016 Jan 20;8(322):322ra9. PMCID: PMC4774245

9. Minikel EV, Karczewski KJ, Martin HC, Cummings BB, Whiffin N, Rhodes D, Alföldi J, Trembath RC, van Heel DA, Daly MJ, Genome Aggregation Database Production Team, Genome Aggregation Database Consortium, Schreiber SL, MacArthur DG. Evaluating drug targets through human loss-of-function genetic variation. Nature. 2020 May;581(7809):459–464. PMCID: PMC7272226

10. Büeler H, Aguzzi A, Sailer A, Greiner RA, Autenried P, Aguet M, Weissmann C. Mice devoid of PrP are resistant to scrapie. Cell. 1993 Jul 2;73(7):1339–1347. PMID: 8100741

11. Büeler H, Raeber A, Sailer A, Fischer M, Aguzzi A, Weissmann C. High prion and PrPSc levels but delayed onset of disease in scrapie-inoculated mice heterozygous for a disrupted PrP gene. Mol Med Camb Mass. 1994 Nov;1(1):19–30. PMCID: PMC2229922

12. Sakaguchi S, Katamine S, Shigematsu K, Nakatani A, Moriuchi R, Nishida N, Kurokawa K, Nakaoke R, Sato H, Jishage K. Accumulation of proteinase K-resistant prion protein (PrP) is restricted by the expression level of normal PrP in mice inoculated with a mouse-adapted strain of the Creutzfeldt-Jakob disease agent. J Virol. 1995 Dec;69(12):7586–7592. PMCID: PMC189697

13. Fischer M, Rülicke T, Raeber A, Sailer A, Moser M, Oesch B, Brandner S, Aguzzi A, Weissmann C. Prion protein (PrP) with amino-proximal deletions restoring susceptibility of PrP knockout mice to scrapie. EMBO J. 1996 Mar 15;15(6):1255–1264. PMCID: PMC450028

14. Mallucci G, Dickinson A, Linehan J, Klöhn PC, Brandner S, Collinge J. Depleting neuronal PrP in prion infection prevents disease and reverses spongiosis. Science. 2003 Oct 31;302(5646):871–874. PMID: 14593181

15. Safar JG, DeArmond SJ, Kociuba K, Deering C, Didorenko S, Bouzamondo-Bernstein E, Prusiner SB, Tremblay P. Prion clearance in bigenic mice. J Gen Virol. 2005 Oct;86(Pt 10):2913–2923. PMID: 16186247

16. Nazor Friberg K, Hung G, Wancewicz E, Giles K, Black C, Freier S, Bennett F, Dearmond SJ, Freyman Y, Lessard P, Ghaemmaghami S, Prusiner SB. Intracerebral Infusion of Antisense Oligonucleotides Into Prion-infected Mice. Mol Ther Nucleic Acids. 2012;1:e9. PMCID: PMC3381600

17. Raymond GJ, Zhao HT, Race B, Raymond LD, Williams K, Swayze EE, Graffam S, Le J, Caron T, Stathopoulos J, O'Keefe R, Lubke LL, Reidenbach AG, Kraus A, Schreiber SL, Mazur C, Cabin DE, Carroll JB, Minikel EV, Kordasiewicz H, Caughey B, Vallabh SM. Antisense oligonucleotides extend survival of prion-infected mice. JCI Insight. 2019 30;5. PMID: 31361599

18. Minikel EV, Zhao HT, Le J, O'Moore J, Pitstick R, Graffam S, Carlson GA, Kavanaugh MP, Kriz J, Kim JB, Ma J, Wille H, Aiken J, McKenzie D, Doh-Ura K, Beck M, O'Keefe R, Stathopoulos J, Caron T, Schreiber SL, Carroll JB, Kordasiewicz HB, Cabin DE, Vallabh SM. Prion protein lowering is a disease-modifying therapy across prion disease stages, strains and endpoints. Nucleic Acids Res. 2020 Aug 10; PMID: 32776089

19. Hay M, Thomas DW, Craighead JL, Economides C, Rosenthal J. Clinical development success rates for investigational drugs. Nat Biotechnol. 2014 Jan;32(1):40–51. PMID: 24406927

20. Wong CH, Siah KW, Lo AW. Estimation of clinical trial success rates and related parameters. Biostat Oxf Engl. 2019 01;20(2):273–286. PMCID: PMC6409418

21. Thomas D, Chancellor D, Micklus A, LaFever S, Hay M, Chaudhuri S, Bowden R, Lo AW. Clinical Development Success Rates and Contributing Factors 2011–2020 [Internet]. 2021 p. 34. Available from: https://go.bio.org/rs/490-EHZ-999/images/ClinicalDevelopmentSuccessRates2011_2020.pdf

22. Minikel EV, Painter JL, Dong CC, Nelson MR. Refining the impact of genetic evidence on clinical success. Nature. 2024 Apr 17; PMID: 38632401

23. Mortberg MA, Vallabh SM, Minikel EV. Disease stages and therapeutic hypotheses in two decades of neurodegenerative disease clinical trials. Sci Rep. 2022 Oct 21;12(1):17708. PMCID: PMC9587287

24. Sandberg MK, Al-Doujaily H, Sharps B, De Oliveira MW, Schmidt C, Richard-Londt A, Lyall S, Linehan JM, Brandner S, Wadsworth JDF, Clarke AR, Collinge J. Prion neuropathology follows the accumulation of alternate prion protein isoforms after infective titre has peaked. Nat Commun. 2014 Jul 9;5:4347. PMCID: PMC4104459

25. Wu H, Lima WF, Zhang H, Fan A, Sun H, Crooke ST. Determination of the role of the human RNase H1 in the pharmacology of DNA-like antisense drugs. J Biol Chem. 2004 Apr 23;279(17):17181–17189. PMID: 14960586

26. Tang Q, Khvorova A. RNAi-based drug design: considerations and future directions. Nat Rev Drug Discov. 2024 May;23(5):341–364. PMCID: PMC11144061

27. Dowdy SF. Endosomal escape of RNA therapeutics: How do we solve this rate-limiting problem? RNA N Y N. 2023 Apr;29(4):396–401. PMCID: PMC10019367

28. Alterman JF, Godinho BMDC, Hassler MR, Ferguson CM, Echeverria D, Sapp E, Haraszti RA, Coles AH, Conroy F, Miller R, Roux L, Yan P, Knox EG, Turanov AA, King RM, Gernoux G, Mueller C, Gray-Edwards HL, Moser RP, Bishop NC, Jaber SM, Gounis MJ, Sena-Esteves M, Pai AA, DiFiglia M, Aronin N, Khvorova A. A divalent siRNA chemical scaffold for potent and sustained modulation of gene expression throughout the central nervous system. Nat Biotechnol. 2019;37(8):884–894. PMCID: PMC6879195

29. Ferguson CM, Hildebrand S, Godinho BMDC, Buchwald J, Echeverria D, Coles A, Grigorenko A, Vangjeli L, Sousa J, McHugh N, Hassler M, Santarelli F, Heneka MT, Rogaev E, Khvorova A. Silencing Apoe with divalent-siRNAs improves amyloid burden and activates immune response pathways in Alzheimer's disease. Alzheimers Dement J Alzheimers Assoc. 2024 Apr;20(4):2632–2652. PMCID: PMC11032532

30. Weiss A, Gilbert JW, Flores IVR, Belgrad J, Ferguson C, Dogan EO, Wightman N, Mocarski K, Echeverria D, Summers A, Bramato B, McHugh N, Furgal R, Yamada N, Cooper D, Monopoli K, Godinho BMDC, Hassler MR, Yamada K, Greer P, Henninger N, Brown RH, Khvorova A. RNAi-mediated silencing of SOD1 profoundly extends survival and functional outcomes in ALS mice. BioRxiv Prepr Serv Biol. 2024 Jun 25;2024.06.20.599943. PMCID: PMC11230209

31. Crooke ST, Vickers TA, Liang XH. Phosphorothioate modified oligonucleotide-protein interactions. Nucleic Acids Res. 2020 Jun 4;48(10):5235–5253. PMCID: PMC7261153

32. Shen W, De Hoyos CL, Migawa MT, Vickers TA, Sun H, Low A, Bell TA, Rahdar M, Mukhopadhyay S, Hart CE, Bell M, Riney S, Murray SF, Greenlee S, Crooke RM, Liang XH, Seth PP, Crooke ST. Chemical modification of PS-ASO therapeutics reduces cellular protein-binding and improves the therapeutic index. Nat Biotechnol. 2019 Jun;37(6):640–650. PMID: 31036929

33. Yamada K, Hariharan VN, Caiazzi J, Miller R, Ferguson CM, Sapp E, Fakih HH, Tang Q, Yamada N, Furgal RC, Paquette JD, Biscans A, Bramato BM, McHugh N, Summers A, Lochmann C, Godinho BMDC, Hildebrand S, Jackson SO, Echeverria D, Hassler MR, Alterman JF, DiFiglia M, Aronin N, Khvorova A. Enhancing siRNA efficacy in vivo with extended nucleic acid backbones. Nat Biotechnol. 2024 Aug 1; PMID: 39090305

34. De N, Young L, Lau PW, Meisner NC, Morrissey DV, MacRae IJ. Highly complementary target RNAs promote release of guide RNAs from human Argonaute2. Mol Cell. 2013 May 9;50(3):344–355. PMCID: PMC3746828

35. Sheu-Gruttadauria J, Pawlica P, Klum SM, Wang S, Yario TA, Schirle Oakdale NT, Steitz JA, MacRae IJ. Structural Basis for Target-Directed MicroRNA Degradation. Mol Cell. 2019 Sep 19;75(6):1243-1255.e7. PMCID: PMC6754277

36. Tang Q, Fakih HH, Zain Ui Abideen M, Hildebrand SR, Afshari K, Gross KY, Sousa J, Maebius AS, Bartholdy C, Søgaard PP, Jackerott M, Hariharan V, Summers A, Fan X, Okamura K, Monopoli KR, Cooper DA, Echeverria D, Bramato B, McHugh N, Furgal RC, Dresser K, Winter SJ, Biscans A, Chuprin J, Haddadi NS, Sherman S, Yıldız-Altay Ü, Rashighi M, Richmond JM, Bouix-Peter C, Blanchard C, Clauss A, Alterman JF, Khvorova A, Harris JE. Rational design of a JAK1-selective siRNA inhibitor for the modulation of autoimmunity in the skin. Nat Commun. 2023 Nov 4;14(1):7099. PMCID: PMC10625637

37. Gentile JE, Corridon TL, Mortberg MA, D'Souza EN, Whiffin N, Minikel EV, Vallabh SM. Modulation of prion protein expression through cryptic splice site manipulation. J Biol Chem. 2024 Aug;300(8):107560. PMCID: PMC11342779

38. Nuvolone M, Hermann M, Sorce S, Russo G, Tiberi C, Schwarz P, Minikel E, Sanoudou D, Pelczar P, Aguzzi A. Strictly co-isogenic C57BL/6J-Prnp-/- mice: A rigorous resource for prion science. J Exp Med. 2016 Mar 7;213(3):313–327. PMCID: PMC4813672

39. de Vree PJP, de Wit E, Yilmaz M, van de Heijning M, Klous P, Verstegen MJAM, Wan Y, Teunissen H, Krijger PHL, Geeven G, Eijk PP, Sie D, Ylstra B, Hulsman LOM, van Dooren MF, van Zutven LJCM, van den Ouweland A, Verbeek S, van Dijk KW, Cornelissen M, Das AT, Berkhout B, Sikkema-Raddatz B, van den Berg E, van der Vlies P, Weening D, den Dunnen JT, Matusiak M, Lamkanfi M, Ligtenberg MJL, ter Brugge P, Jonkers J, Foekens JA, Martens JW, van der Luijt R, van Amstel HKP, van Min M, Splinter E, de Laat W. Targeted sequencing by proximity ligation for comprehensive variant detection and local haplotyping. Nat Biotechnol. 2014 Oct;32(10):1019–1025. PMID: 25129690

40. Vallabh SM, Minikel EV, Williams VJ, Carlyle BC, McManus AJ, Wennick CD, Bolling A, Trombetta BA, Urick D, Nobuhara CK, Gerber J, Duddy H, Lachmann I, Stehmann C, Collins SJ, Blennow K, Zetterberg H, Arnold SE. Cerebrospinal fluid and plasma biomarkers in individuals at risk for genetic prion disease. BMC Med. 2020 Jun 18;18(1):140. PMCID: PMC7302371

41. Miller R, Paquette J, Barker A, Sapp E, McHugh N, Bramato B, Yamada N, Alterman J, Echeveria D, Yamada K, Watts J, Anaclet C, DiFiglia M, Khvorova A, Aronin N. Preventing acute neurotoxicity of CNS therapeutic oligonucleotides with the addition of Ca2+ and Mg2+ in the formulation. Mol Ther Nucleic Acids. 2024 Dec 10;35(4):102359. PMCID: PMC11567125

42. Moazami MP, Rembetsy-Brown JM, Sarli SL, McEachern HR, Wang F, Ohara M, Wagh A, Kelly K, Krishnamurthy PM, Weiss A, Marosfoi M, King RM, Motwani M, Gray-Edwards H, Fitzgerald KA, Brown RH, Watts JK. Quantifying and mitigating motor phenotypes induced by antisense oligonucleotides in the central nervous system. Mol Ther J Am Soc Gene Ther. 2024 Oct 28;S1525-0016(24)00684–1. PMID: 39460376

43. Jones S. Avertin Solution for Mouse Anesthesia [Internet]. UMass Medical School; [cited 2024 Apr 17]. Available from: https://web.archive.org/web/20240417142838/https://www.umassmed.edu/globalassets/cell-and-developmental-biology-labs/jones-lab/files/protocols/avertin.pdf

44. Corridon TL, O'Moore J, Lian Y, Laversenne V, Noble B, Kamath NG, Serack FE, Shaikh AB, Erickson B, Braun C, Lenz K, Howard M, Chan N, Reidenbach AG, Cabin DE, Vallabh SM, Grindeland A, Oberbeck N, Zhao HT, Minikel EV. PrP turnover in vivo and the time to effect of prion disease therapeutics. bioRxiv. 2024 Nov 14;2024.11.12.623215.

45. Chandler RL. Encephalopathy in mice produced by inoculation with scrapie brain material. Lancet Lond Engl. 1961 Jun 24;1(7191):1378–1379. PMID: 13692303

46. Mortberg MA, Zhao HT, Reidenbach AG, Gentile JE, Kuhn E, O'Moore J, Dooley PM, Connors TR, Mazur C, Allen SW, Trombetta BA, McManus A, Moore MR, Liu J, Cabin DE, Kordasiewicz HB, Mathews J, Arnold SE, Vallabh SM, Minikel EV. Regional variability and genotypic and pharmacodynamic effects on PrP concentration in the CNS. JCI Insight. 2022 Mar 22;7(6):e156532. PMCID: PMC8986079

47. Reidenbach AG, Mesleh MF, Casalena D, Vallabh SM, Dahlin JL, Leed AJ, Chan AI, Usanov DL, Yehl JB, Lemke CT, Campbell AJ, Shah RN, Shrestha OK, Sacher JR, Rangel VL, Moroco JA, Sathappa M, Nonato MC, Nguyen KT, Wright SK, Liu DR, Wagner FF, Kaushik VK, Auld DS, Schreiber SL, Minikel EV. Multimodal small-molecule screening for human prion protein binders. J Biol Chem. 2020 Sep 25;295(39):13516–13531. PMCID: PMC7521658

48. Ritz C, Baty F, Streibig JC, Gerhard D. Dose-Response Analysis Using R. PloS One. 2015;10(12):e0146021. PMCID: PMC4696819

49. Khvorova A, Kennedy Z. Oligonucleotides for prnp modulation [Internet]. US20210317460, 2021 [cited 2022 Sep 21]. Available from: https://patents.google.com/patent/US20210317460A1/en?oq=US+2021%2f0317460+A1

50. Tang T, Li L, Tang J, Li Y, Lin WY, Martin F, Grant D, Solloway M, Parker L, Ye W, Forrest W, Ghilardi N, Oravecz T, Platt KA, Rice DS, Hansen GM, Abuin A, Eberhart DE, Godowski P, Holt KH, Peterson A, Zambrowicz BP, de Sauvage FJ. A mouse knockout library for secreted and transmembrane proteins. Nat Biotechnol. 2010 Jul;28(7):749–755. PMID: 20562862

51. Dickinson ME, Flenniken AM, Ji X, Teboul L, Wong MD, White JK, Meehan TF, Weninger WJ, Westerberg H, Adissu H, Baker CN, Bower L, Brown JM, Caddle LB, Chiani F, Clary D, Cleak J, Daly MJ, Denegre JM, Doe B, Dolan ME, Edie SM, Fuchs H, Gailus-Durner V, Galli A, Gambadoro A, Gallegos J, Guo S, Horner NR, Hsu CW, Johnson SJ, Kalaga S, Keith LC, Lanoue L, Lawson TN, Lek M, Mark M, Marschall S, Mason J, McElwee ML, Newbigging S, Nutter LMJ, Peterson KA, Ramirez-Solis R, Rowland DJ, Ryder E, Samocha KE, Seavitt JR, Selloum M, Szoke-Kovacs Z, Tamura M, Trainor AG, Tudose I, Wakana S, Warren J, Wendling O, West DB, Wong L, Yoshiki A, International Mouse Phenotyping Consortium, Jackson Laboratory, Infrastructure Nationale PHENOMIN, Institut Clinique de la Souris (ICS), Charles River Laboratories, MRC Harwell, Toronto Centre for Phenogenomics, Wellcome Trust Sanger Institute, RIKEN BioResource Center, MacArthur DG, Tocchini-Valentini GP, Gao X, Flicek P, Bradley A, Skarnes WC, Justice MJ, Parkinson HE, Moore M, Wells S, Braun RE, Svenson KL, de Angelis MH, Herault Y, Mohun T, Mallon AM, Henkelman RM, Brown SDM, Adams DJ, Lloyd KCK, McKerlie C, Beaudet AL, Bućan M, Murray SA. High-throughput discovery of novel developmental phenotypes. Nature. 2016 Sep 22;537(7621):508–514. PMCID: PMC5295821

52. Frmd6 | FERM domain containing 6 mouse gene | IMPC [Internet]. International Mouse Phenotyping Consortium (IMPC). [cited 2024 Nov 8]. Available from: https://dev.mousephenotype.org/data/genes/MGI:2442579

53. Schirle NT, Sheu-Gruttadauria J, MacRae IJ. Structural basis for microRNA targeting. Science. 2014 Oct 31;346(6209):608–613. PMCID: PMC4313529

54. Becker WR, Ober-Reynolds B, Jouravleva K, Jolly SM, Zamore PD, Greenleaf WJ. High-Throughput Analysis Reveals Rules for Target RNA Binding and Cleavage by AGO2. Mol Cell. 2019 Aug 22;75(4):741-755.e11. PMCID: PMC6823844

55. Wang PY, Bartel DP. The guide-RNA sequence dictates the slicing kinetics and conformational dynamics of the Argonaute silencing complex. Mol Cell. 2024 Aug 8;84(15):2918-2934.e11. PMCID: PMC11371465

56. Freier SM, Bui HH, Zhao H. Compounds and methods for reducing prion expression [Internet]. WO2020106996A1, 2020 [cited 2021 Jan 22]. Available from: https://patents.google.com/patent/WO2020106996A1/en

57. Emami A, Tepper J, Short B, Yaksh TL, Bendele AM, Ramani T, Cisternas AF, Chang JH, Mellon RD. Toxicology Evaluation of Drugs Administered via Uncommon Routes: Intranasal, Intraocular, Intrathecal/Intraspinal, and Intra-Articular. Int J Toxicol. 2018;37(1):4–27. PMCID: PMC5874330

58. Stern S, Wange RL, Rogers H. An Evaluation of First-in-Human Studies for RNA Oligonucleotides. Nucleic Acid Ther. 2024 Sep 23; PMID: 39311689

59. Miller TM, Cudkowicz ME, Genge A, Shaw PJ, Sobue G, Bucelli RC, Chiò A, Van Damme P, Ludolph AC, Glass JD, Andrews JA, Babu S, Benatar M, McDermott CJ, Cochrane T, Chary S, Chew S, Zhu H, Wu F, Nestorov I, Graham D, Sun P, McNeill M, Fanning L, Ferguson TA, Fradette S, VALOR and OLE Working Group. Trial of Antisense Oligonucleotide Tofersen for SOD1 ALS. N Engl J Med. 2022 Sep 22;387(12):1099–1110. PMID: 36129998

60. McDonough S. Widespread and Durable Knockdown of HTT in Non-Human Primate Brain by a Novel Oligonucleotide Modality. Palm Springs, CA; Available from: https://www.atalantatx.com/wp-content/uploads/CHDI-Poster-2024.pdf]

61. Ferguson CM, Godinho BM, Alterman JF, Coles AH, Hassler M, Echeverria D, Gilbert JW, Knox EG, Caiazzi J, Haraszti RA, King RM, Taghian T, Puri A, Moser RP, Gounis MJ, Aronin N, Gray-Edwards H, Khvorova A. Comparative route of administration studies using therapeutic siRNAs show widespread gene modulation in Dorset sheep. JCI Insight. 2021 Dec 22;6(24):e152203. PMCID: PMC8783676

62. Jafar-Nejad P, Powers B, Soriano A, Zhao H, Norris DA, Matson J, DeBrosse-Serra B, Watson J, Narayanan P, Chun SJ, Mazur C, Kordasiewicz H, Swayze EE, Rigo F. The atlas of RNase H antisense oligonucleotide distribution and activity in the CNS of rodents and non-human primates following central administration. Nucleic Acids Res. 2021 Jan 25;49(2):657–673. PMCID: PMC7826274

63. Brandel JP, Vlaicu MB, Culeux A, Belondrade M, Bougard D, Grznarova K, Denouel A, Plu I, Bouaziz-Amar E, Seilhean D, Levasseur M, Haïk S. Variant Creutzfeldt-Jakob Disease Diagnosed 7.5 Years after Occupational Exposure. N Engl J Med. 2020 02;383(1):83–85. PMID: 32609989

64. Casassus B. France halts prion research amid safety concerns. Science. 2021 Jul 30;373(6554):475–476. PMID: 34326214

Supplement

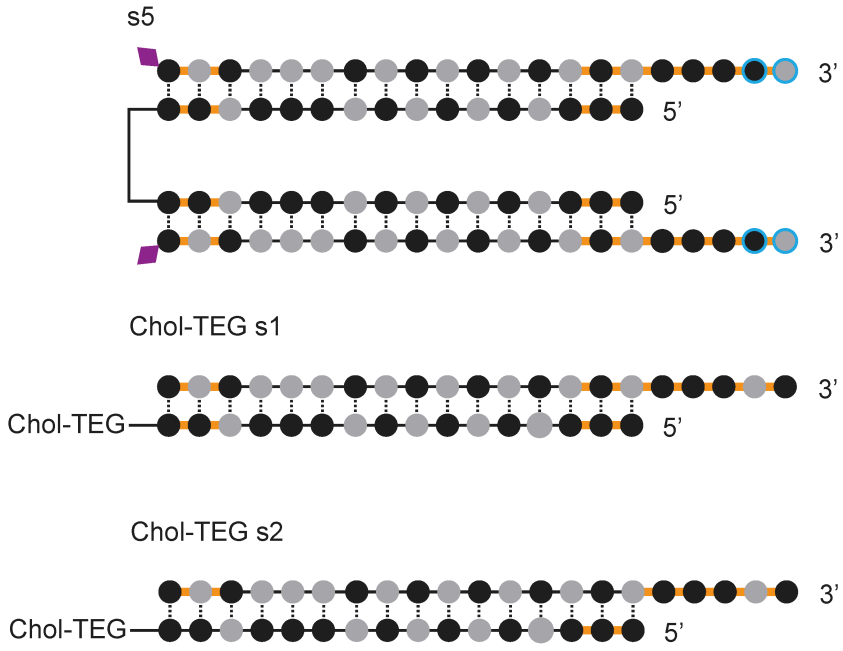

Figure S1. Additional chemical scaffolds. *Scaffold s5 is utilized in Figure S8. The Chol-TEG scaffolds were used in screening in figures*

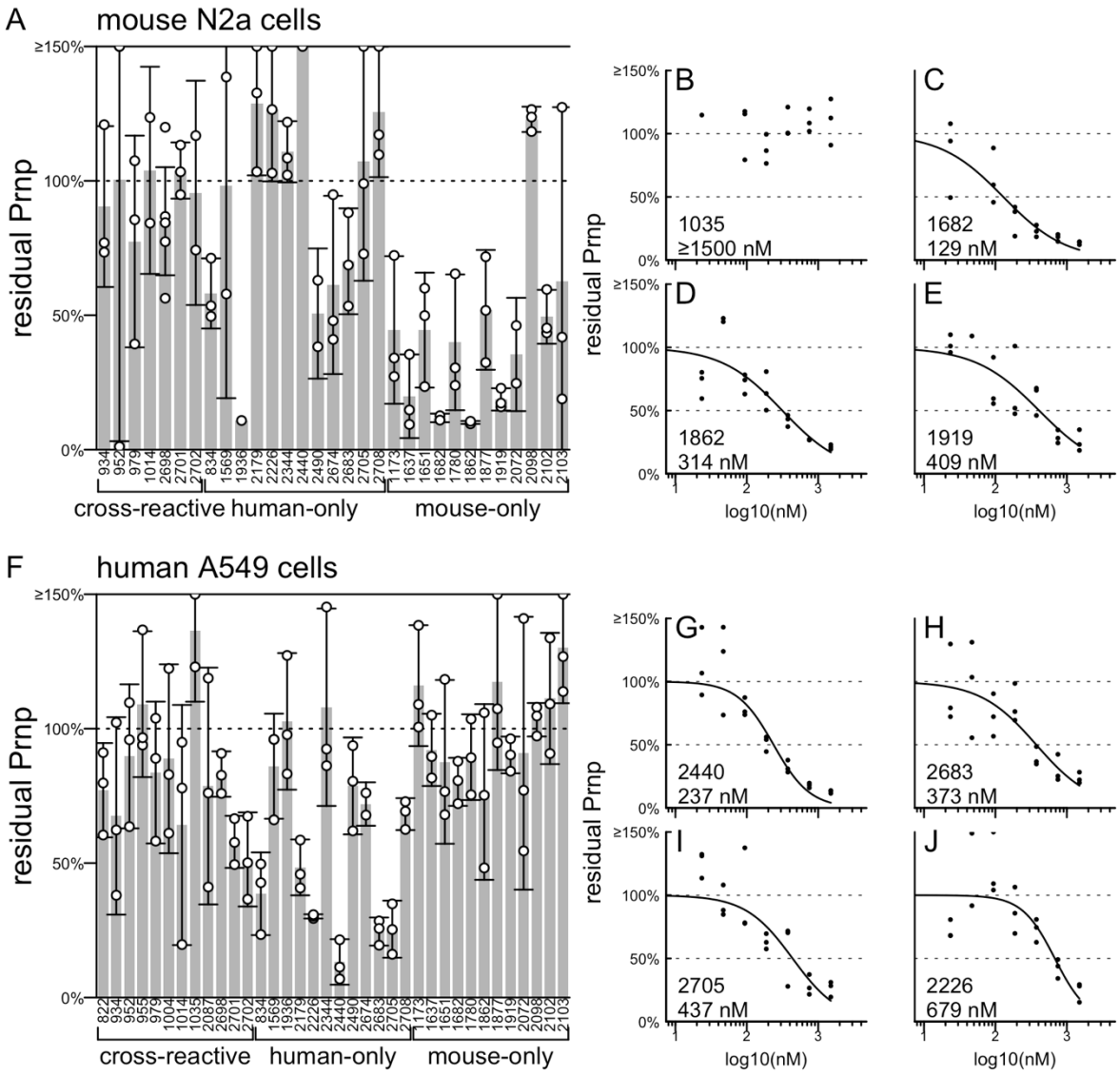

Figure S2. Initial screening by bDNA assay in cell culture. *These screens used scaffold Chol-TEG s1 (Figure S1).* ***A)*** *Mouse N2a cells, each point is one well, triplicate wells are analyzed for each compound, rectangular bars are means, error bars are 95% confidence intervals. Readout is Prnp expression normalized to Hprt, further normalized to the mean of predicted non-targeting (human-only) compounds.* ***B-E)*** *IC_{50} determination for 4 compounds selected from mouse N2a cell screen. Each point is one well, triplicate wells are tested at each dose level, curves are 4-parameter log-logistic dose-response curves fit using the drc package in R.* ***F)*** *As in (A) but for human A549 cells.* ***G-J)*** *As in (B-E) but for top human sequences in human A549 cells.*

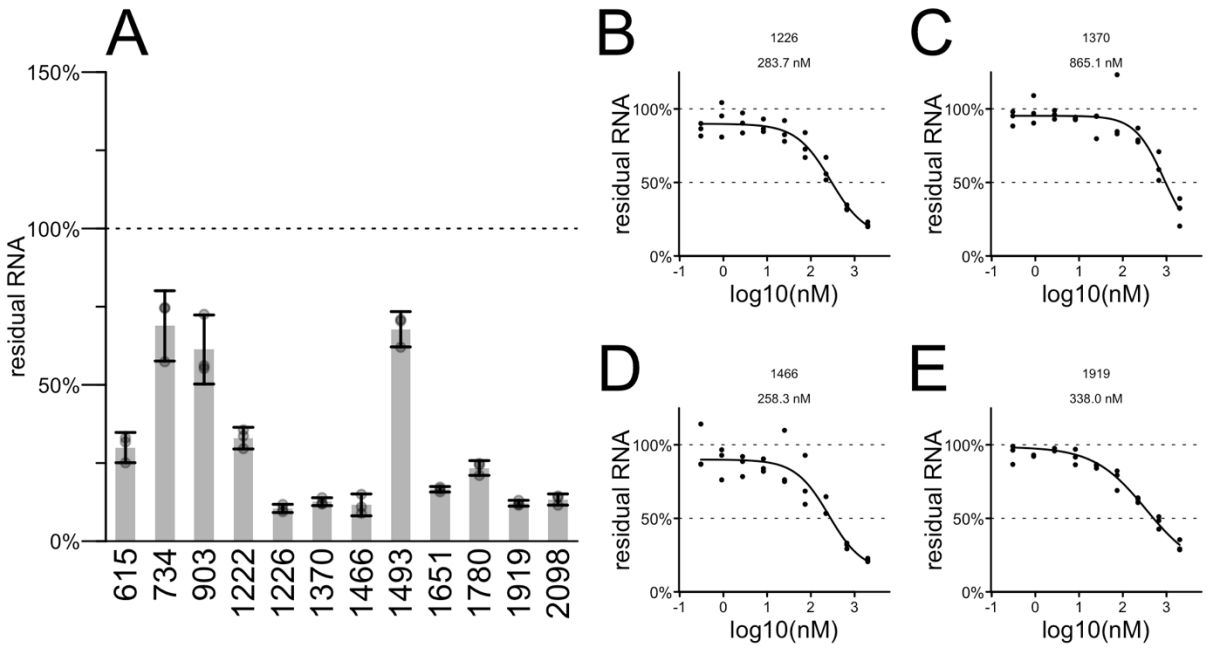

Figure S3. Further screening of potential siRNA tool compounds against mouse Prnp in N2a cells. *This screen used scaffold Chol-TEG s2 (Figure S1).* ***A)*** *Each point is one well, triplicate wells are analyzed for each compound, readout is qPCR with Prnp Ct values normalized to Tbp, then each point is normalized to the mean of untreated wells. Rectangular bars are means, error bars are 95% confidence intervals.* ***B-E)*** *IC_{50} determination for top compounds. Each point is one well, triplicate wells are tested at each dose level, curves are 4-parameter log-logistic dose-response curves fit using the drc package in R.*

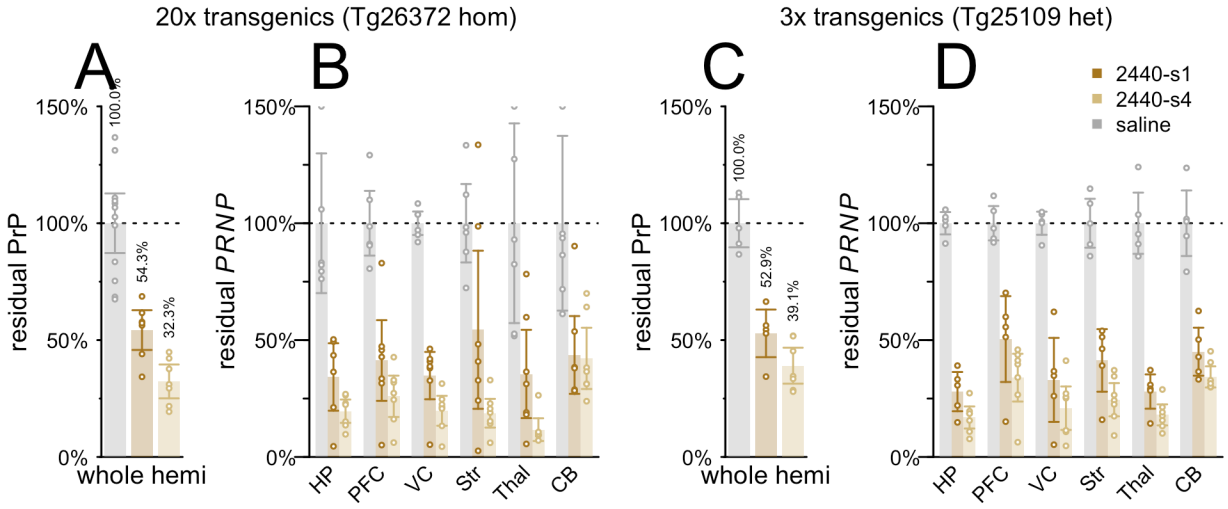

Figure S4. Potency of tool compound 2440 in high or low copy number HuPrP transgenic mice. A-B) *2440-s1 and 2440-s4 tested at 348 µg in Tg26372 homozygous mice with 20 copies of PRNP and 5.4x PrP expression.* ***A)*** *Whole hemisphere PrP ELISA readout. These data are reproduced from Figure 4C for convenience of comparison.* ***B)*** *Regional qPCR readout.* ***C-D)*** *2440-s1 and 2440-s4 tested at 348 µg in Tg25109 heterozygous mice with 3 copies of PRNP*

and 1.1x PrP expression. ***C)*** *Whole hemisphere PrP ELISA readout.* ***D)*** *Regional qPCR readout. For all panels, each point is one animal, rectangular bars are means, error bars are 95% confidence intervals.*

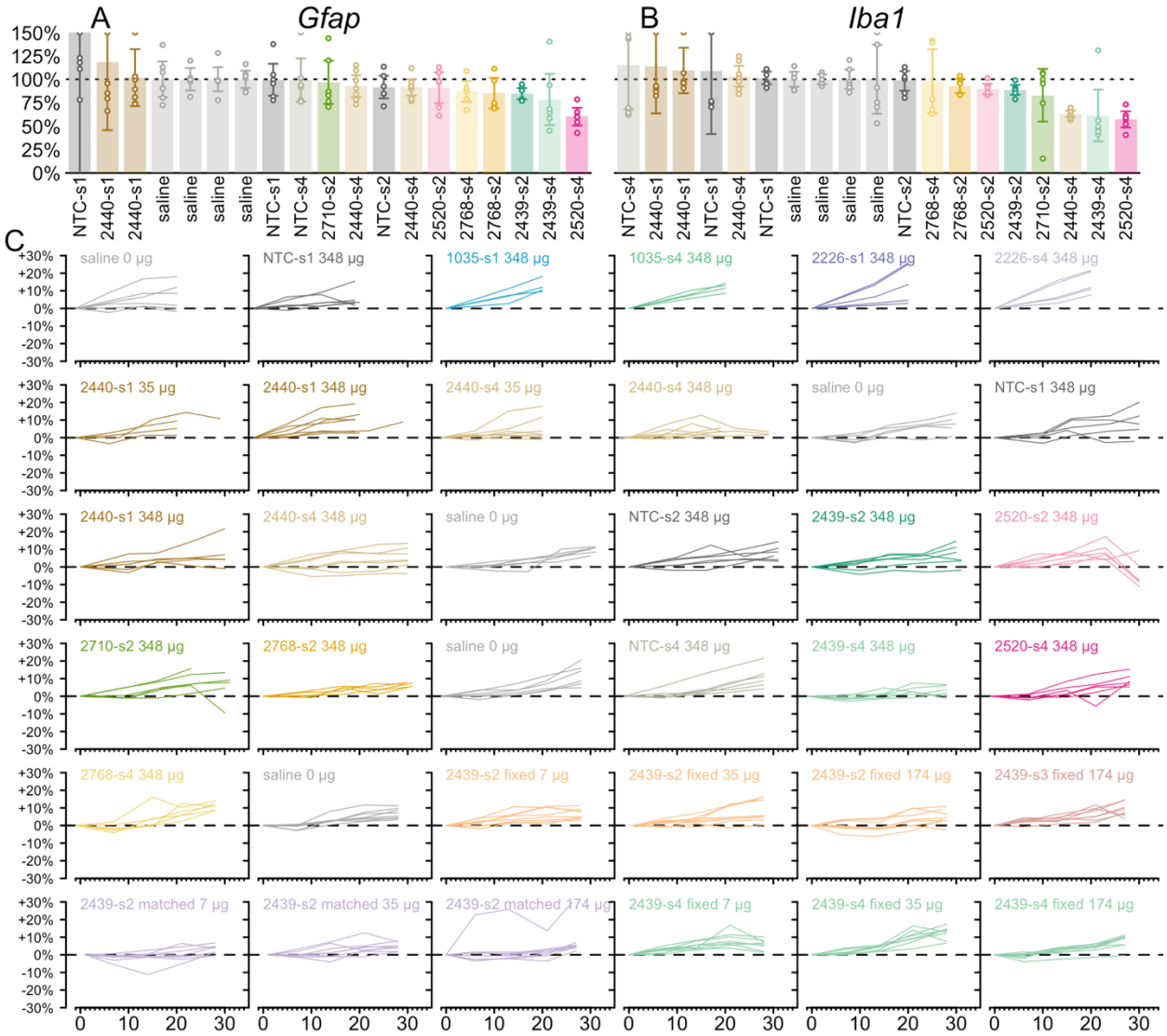

Figure S5. Tolerability metrics for divalent siRNAs in short-term target engagement studies. A) *Gfap and* ***B)*** *Iba1 by qPCR in visual cortex for all studies in Figure 4 and Figure 5, normalized to the mean of saline controls within each study. Each point is one animal. Rectangular bars are means, error bars are 95% confidence intervals. Compounds are sorted along the x axis by rank of mean expression of each inflammatory marker.* ***C)*** *Individual weight gain trajectories for every animal in Figure 4 and 5, normalized to individual baseline. Weight change from individual baseline as a percent (y axis) versus days post-dose (x axis).*

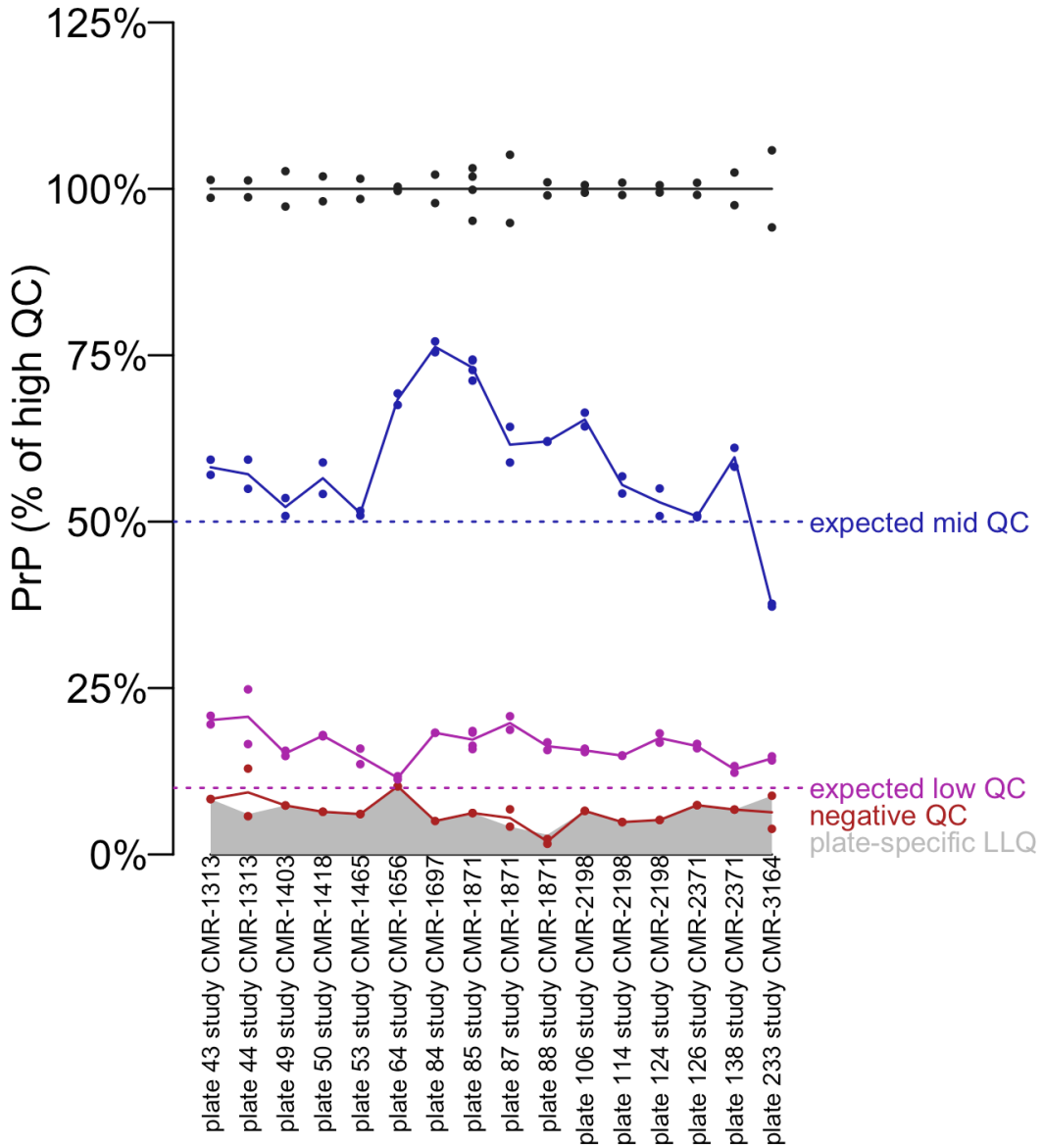

Figure S6. Quality control metrics for PrP ELISA plates. *Every plate includes, in duplicate, the same high QC (WT mouse brain, black), mid QC (het KO mouse brain, blue), low QC (contrived sample of 90% KO brain homogenate spiked with 10% WT brain homogenate to simulate 10% residual PrP, magenta) and negative QC (KO brain, maroon). The LLQ is 0.05 ng/mL, and QCs are run at a final 1:200 dilution so that 10 ng PrP per g of wet brain tissue is the lower limit of quantification for these samples. In this plot, each point is one replicate of a QC, and its PrP concentration is normalized to the mean of high QCs. Readings from consecutive plates are connected by lines.*

A

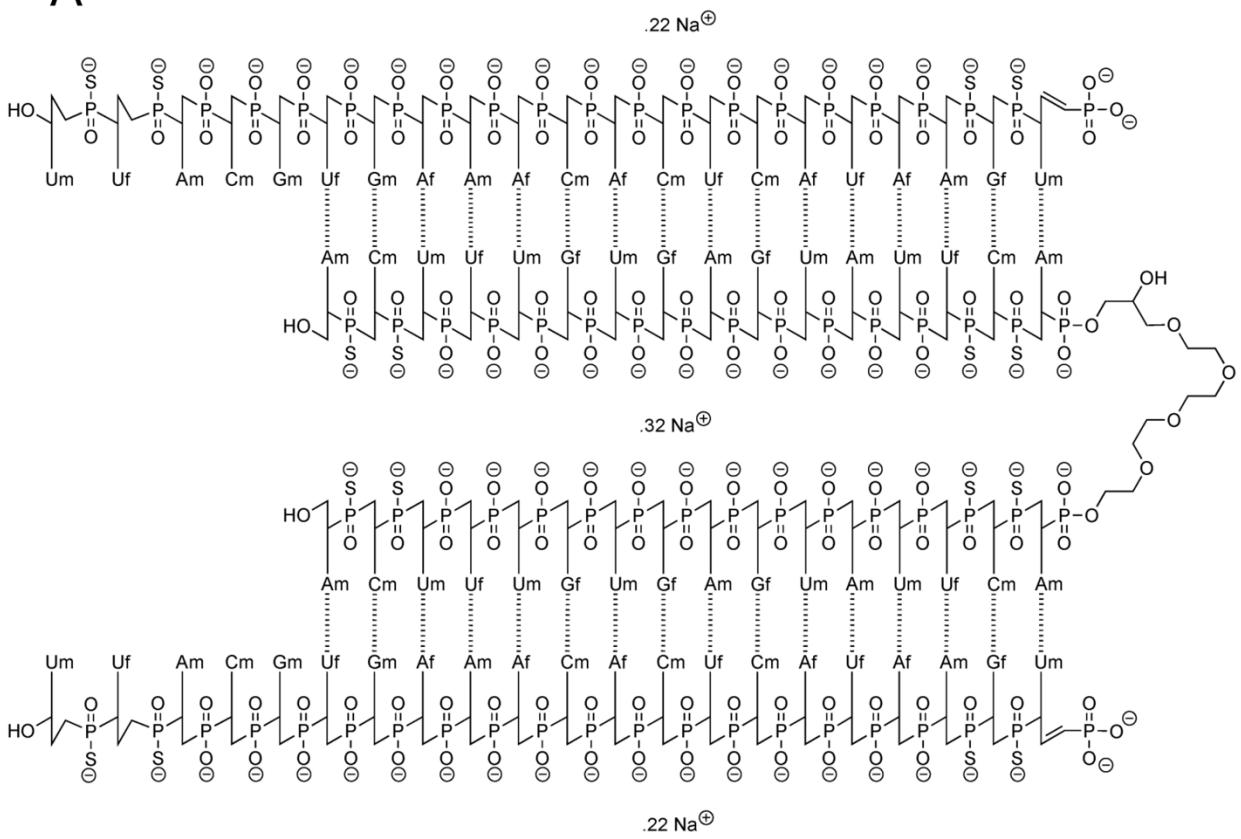

B

human	**CACTTTGTGAGTATTC**
rhesus	**CACTTTGTGAGTATTC**
cynomolgus	**CACTTTGTGAGTATTC**
marmoset	CACTTTGTGAGTATTT
squirrel monkey	CACTTTGTGAGTATTT
spider monkey	CACTTTGTGAGTATTT
sheep	CACCTTGTG-GTATCC
pig	CACTTTGTGGGTATCC

Figure S7. Identity and cross-species reactivity analysis for sequence 2439. A) *Chemical structure of 2439-s4. f = 2' Fluoro, m = 2'-O-methyl.* ***B)*** *Multiple species alignment of genomic sequences complementing bases 2-17 of the antisense strand. Fully matched sequences are shown in bold black. For imperfectly matched species, matched bases in black, indels or mismatches in red. No alignments were found for mouse, rat, Syrian hamster, or dog.*

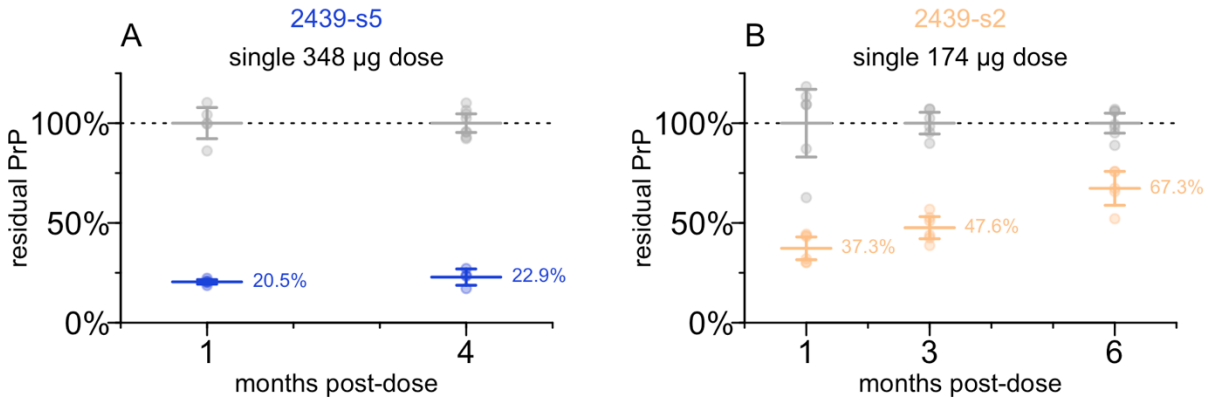

Figure S8. Durability studies for 2439 in other scaffolds. A) *2439-s5 (see Figure S1 for scaffold description) at 348 µg.* ***B)*** *2439-s2 at 174 µg. The same control animals from Figure 6 are reproduced here for convenience of comparison.*

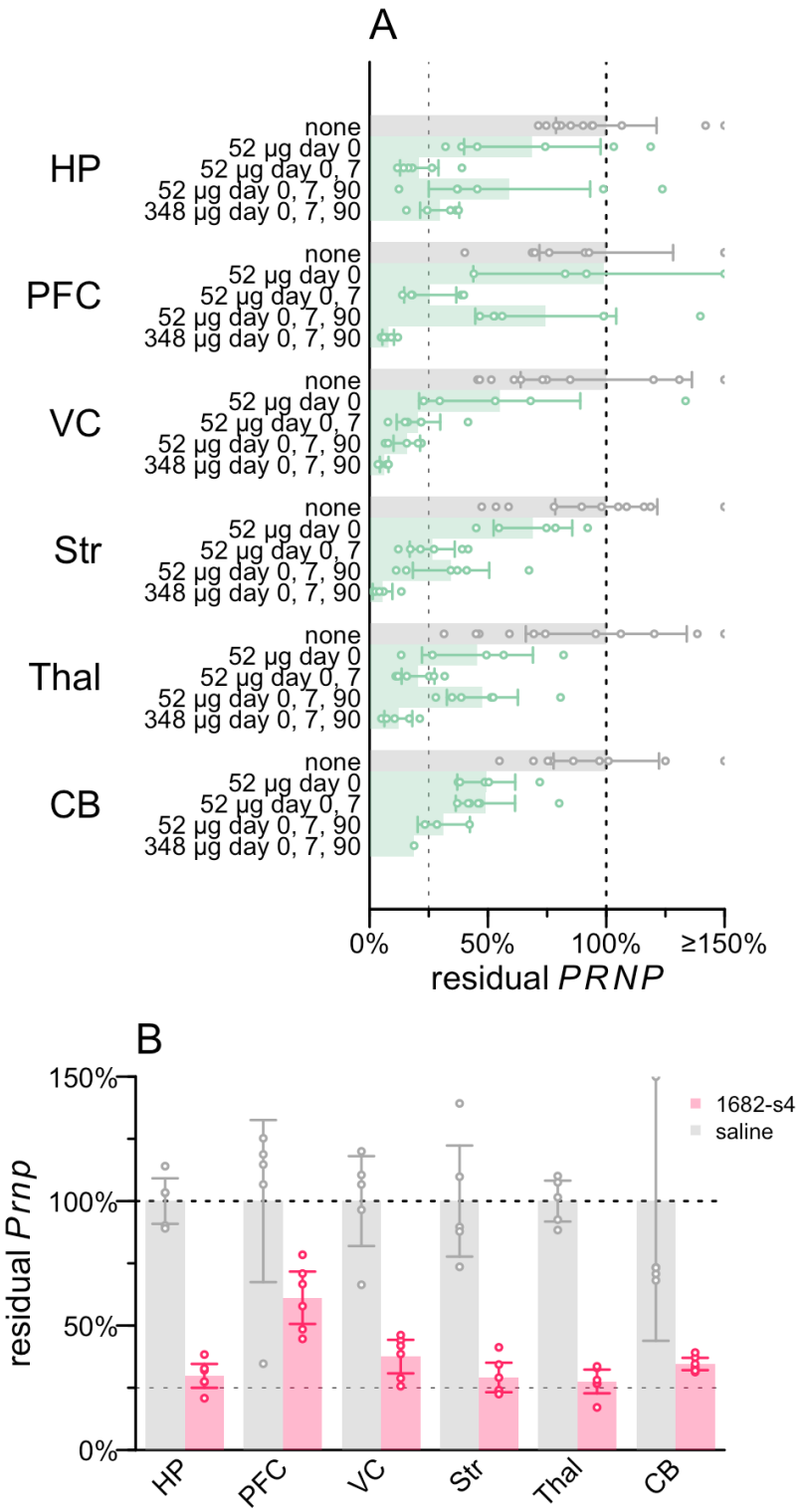

Figure S9. Regional qPCR analysis for repeat dose 2439-s4 versus 1682-s4. *Regions: hippocampus (HP), prefrontal cortex (PFC), visual cortex (VC), striatum (Str), thalamus (Thal), and cerebellum (CB).* ***A)*** *Regional PRNP qPCR analysis for repeat dose 2439-s4 study in the same Tg26372 animals shown in Figure 6D.* ***B)*** *Regional Prnp qPCR for 1682-s4 from the same animals shown in Figure 2A.*